Author Manuscript

Author Manuscript

Author Manuscript

Author Manuscript

HHS Public Access

Author manuscript

Dev Cell. Author manuscript; available in PMC 2019 July 16.

Published in final edited form as:

Dev Cell. 2018 July 16; 46(2): 219–235.e8. doi:10.1016/j.devcel.2018.06.016.

Global proteome remodeling during ER stress involves Hac1-driven expression of long undecoded transcript isoforms

Kelsey Marie Van Dalfsen[1], **Stefanie Hodapp**[2], **Abdurrahman Keskin**[2], **George Maxwell Otto**[1], **Charles Andrew Berdan**[3], **Andrea Higdon**[1], **Tia Cheunkarndee**[1], **Daniel Koji Nomura**[1,3], **Marko Jovanovic**[2], and **Gloria Ann Brar**[1,*,‡]

[1]Department of Molecular and Cell Biology, University of California, Berkeley, CA, 94720, USA

[2]Department of Biological Sciences, Columbia University, New York, NY, 10027, USA

[3]Departments of Chemistry and Nutritional Sciences and Toxicology, University of California, Berkeley, California 94720, USA

Summary:

Cellular stress responses often require transcription-based activation of gene expression to promote cellular adaptation. Whether general mechanisms exist for stress-responsive gene down-regulation is less clear. A recently defined mechanism enables both up- *and* down-regulation of protein levels for distinct gene sets by the same transcription factor (TF) via coordinated induction of canonical mRNAs and long undecoded transcript isoforms (LUTIs). We analyzed parallel gene expression datasets to determine whether this mechanism contributes to the conserved Hac1-driven branch of the unfolded protein response (UPR^{ER}), indeed observing Hac1-dependent protein down-regulation accompanying the up-regulation of ER-related proteins that typifies UPR^{ER} activation. Proteins down-regulated by Hac1-driven LUTIs include those with electron transport chain (ETC) function. Abrogated ETC function improves the fitness of UPR^{ER}-activated cells, suggesting functional importance to this regulation. We conclude that the UPR^{ER} drives large-scale proteome remodeling, including coordinated up- and down-regulation of distinct protein classes, which is partly mediated by Hac1-induced LUTIs.

Abstract

*Corresponding Author: gabrar@berkeley.edu.
‡Lead Contact

Author Contributions:

K.M.V. and G.A.B conceived the study. Sequencing experiments were performed by K.M.V. and G.A.B. Protein mass spectrometry was performed by S.H., A.K., and M.J. Metabolite analyses were performed by C.B. All other experiments were performed by K.M.V. with assistance from T.C. and G.M.O. Data analysis was performed by K.M.V., C.B., D.K.N., M.J., A.H., and G.A.B. K.M.V. and G.A.B. wrote and edited the manuscript.

Declaration of Interests:

All authors declare no competing interests.

Publisher's Disclaimer: This is a PDF file of an unedited manuscript that has been accepted for publication. As a service to our customers we are providing this early version of the manuscript. The manuscript will undergo copyediting, typesetting, and review of the resulting proof before it is published in its final citable form. Please note that during the production process errors may be discovered which could affect the content, and all legal disclaimers that apply to the journal pertain.

Author Manuscript Author Manuscript Author Manuscript Author Manuscript

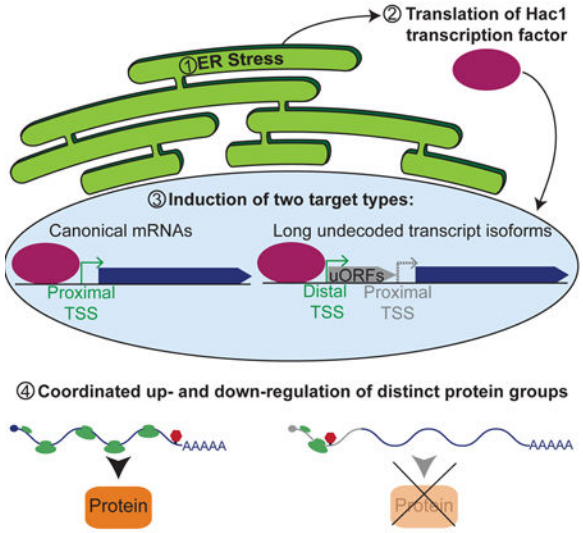

eTOC blurb

Van Dalfsen et al. demonstrate that conserved yeast transcription factor Hac1/XBP1 directs the ER unfolded protein response (UPR^{ER}) not only by gene activation but also coordinate gene repression through a mechanism of long undecoded transcript isoforms (LUTI) production. Via LUTI, Hac1 directs proteome remodeling and influences cellular metabolism control.

Introduction:

Gene regulatory programs are key drivers of cellular state change. The most common class of such programs are transcriptional, in which one or a few transcription factors (TFs) are activated in response to an environmental or developmental cue to induce expression of genes whose protein products are required to promote the transition to a new cell state. It seems likely that such cellular transitions should also require down-regulation of gene sets, either because specific proteins impede the cell's transition to a new cellular state or simply for the cell to free up capacity for the production of proteins needed for the transition. The mechanisms by which such down-regulation is achieved have been less well studied than those that drive up-regulation, although some such mechanisms are known, including those involving protein degradation and transcriptional repressor proteins. With few exceptions [for example (Haghighat et al., 1996; Hinnebusch, 1993; Hollien et al., 2009)], however, our understanding of the gene regulatory programs underlying cellular state change has lacked a coherent explanation for how up- and down-regulation are *coordinated*.

A recently defined mode of gene regulation is an attractive candidate for broadly mediating such coordination (Fig. 1A). This mechanism was shown to harness transcription factor (TF)-driven synthesis of an ORF-encoding transcript to repress synthesis of the kinetochore protein Ndc80, a key event during meiotic differentiation in budding yeast (Chen et al., 2017; Chia et al., 2017). In short, it was found that *NDC80* has two transcription start sites (TSSes) that are activated by different TFs. Activation of the proximal TSS produces a canonical transcript that is translated to produce protein. Activation of the distal TSS results

Author Manuscript Author Manuscript Author Manuscript Author Manuscript

in synthesis of a 5' extended transcript that encodes the *NDC80* ORF, but does not translate it because of translation of uORFs in the extended 5' leader. Use of the distal TSS also represses use of the proximal TSS in cis by transcriptional interference. Effectively, as a result of this integrated mechanism, synthesis of the longer transcript halts Ndc80 protein production. This longer mRNA was termed a "LUTI", for long undecoded transcript isoform (Chen et al., 2017; Chia et al., 2017).

Subsets of the hallmarks of LUTI-based regulation defined above were previously observed for several other genes (Law et al., 2005; Moseley et al., 2002; Sehgal et al., 2008), suggesting that use of this mechanism might be widespread. We recently found that LUTI-based regulation is common and responsible for setting protein levels of at least 380 genes as yeast cells progress through meiotic differentiation (Cheng et al., 2018). We showed that this mechanism enables a single meiotic TF to regulate two distinct sets of targets in a highly coordinated manner. The canonical set includes "positive" targets, whose transcription results in increased protein production, and "negative" LUTI targets, whose transcription leads to decreased protein production. While both sets of targets may exhibit increases in mRNA production, for genes that are regulated by the LUTI-based mechanism, overall mRNA levels are decoupled from protein levels. In fact, the 380 meiotic LUTI targets that we defined were found based on the signature of a poor, or even negative, correlation between mRNA and protein levels over time (Cheng et al., 2018; Otto and Brar, 2018). For these cases, it is the *type* of transcript produced rather than the amount that determines whether protein is synthesized.

Given the pervasiveness of LUTI-based regulation during meiosis, it seemed possible that this mechanism might generally be used to coordinate gene up- and down-regulation during cellular transitions. We sought a well-defined cellular state change in which to test this hypothesis. We chose to focus on the branch of the endoplasmic reticulum unfolded protein response (UPR^{ER}) that is conserved from budding yeast to human and relies on the Hac1 transcription factor (orthologous to Xbp1 in metazoans) to allow cells to respond to aberrant protein folding within the ER lumen [reviewed in (Han and Kaufman, 2017; Walter and Ron, 2011)]. The UPR^{ER} is typically experimentally induced by treatment of cells with drugs that disrupt ER folding, such as dithiothreitol (DTT) or tunicamycin (Tm). The resulting accumulation of misfolded proteins in the ER lumen promotes activation of the ER membrane-spanning kinase Ire1, which subsequently removes a translationally repressive cytoplasmically retained intron from the *HAC1* transcript through an atypical splicing event (Cox and Walter, 1996; Mori et al., 1996; Sidrauski et al., 1996). Spliced *HAC1* mRNA can be efficiently translated to produce a TF that activates a set of target genes, the most well-studied of which play clear roles in increasing ER volume, folding capacity, and quality control. Included in this set of canonical Hac1 targets are chaperones, such as BiP (*KAR2* in yeast), protein disulfide isomerase (*PDI1* in yeast), luminal Hsp70 (*LHS1*), as well as genes responsible for ER structure, lipid synthesis, and ER redox balance, like thiol oxidase [*ERO1*; reviewed in (Chapman et al., 1998)].

An ORF microarray study identified ~400 mRNAs that were induced in response to UPR^{ER} activation in a Hac1-dependent manner, some of which were known to have clear function in ER biology, but many of which were not and whose function in the UPR^{ER} remains

Author Manuscript Author Manuscript Author Manuscript Author Manuscript

mysterious (Travers et al., 2000). Given that mRNA sequence levels can be misleading predictors of gene expression output, we hypothesized that some of the previously identified Hac1 transcriptional targets might actually be negatively regulated at the protein level via a LUTI-based mechanism. If this were true, it might help to explain why many of the genes that are transcriptionally induced by the UPR^{ER} do not result in protein misfolding in the ER when deleted and why—with few exceptions—roles in the UPR^{ER} remain undefined for most (Jonikas et al., 2009; Schuldiner and Weissman, 2013; Travers et al., 2000).

Through analysis of deep, parallel gene expression datasets, we found examples of previously defined Hac1 targets that display *decreased* protein production as a result of UPR^{ER} activation. We expanded our study beyond previously defined targets to identify 15 LUTI targets of Hac1. To enable robust detection of Hac1 targets, we developed a version of this TF that can be conditionally degraded. Using cells carrying this conditional allele, as well as wild-type (WT) and *hac1Δ* cells, we performed thorough profiling of gene expression-measuring mRNA, translation, and protein levels in response to UPR^{ER} activation, with or without Hac1. This allowed us to holistically define the Hac1-dependent cellular response to UPR^{ER} activation, which we found involves coordinated up- and down-regulation of distinct protein groups. We observed, as expected, that protein synthesis and levels of ER proteins are increased upon UPR^{ER} activation. We also observed down-regulation of ribosomal genes, as well as of genes involved in aerobic respiration. In the case of the latter group, observed protein expression decreases were partly controlled by Hac1-induced transcription of LUTI targets. Crippled aerobic respiration was found to provide a growth advantage to UPR^{ER}-induced cells, suggesting a cellular function for UPR^{ER}-mediated gene down-regulation, and raising the possibility that a shift in cellular metabolism is a core part of the UPR^{ER}, at least in yeast. Our results suggest that LUTI-based regulation is a broadly used mechanism by which transcription factors coordinate up- and down-regulation of target genes during cellular state changes.

Results:

Hac1 induces expression of LUTI targets, resulting in protein down-regulation

To determine whether Hac1 induces LUTI-like repressive transcripts as part of the UPR^{ER}, we performed global gene expression measurements in WT and *hac1Δ* cells. We performed parallel mRNA-seq and ribosome profiling on untreated samples and those treated for 1 hr with either DTT or Tm to assay mRNA abundance and translation in response to UPR^{ER} activation (Fig. 1B). We reasoned that canonical Hac1 targets should show a Hac1-dependent increase in both mRNA and translation with DTT or Tm treatment. In contrast, Hac1 LUTI targets may show an increase in mRNA, but regardless of mRNA-level changes, should show a Hac1-dependent *decrease* in translation efficiency [TE; (ribosome footprint RPKM)/(mRNA RPKM)] with UPR^{ER} activation. The set of transcripts reported to be induced by Hac1 based on microarray analyses (Travers et al., 2000) were also generally induced at the mRNA level in our dataset, dependent on Hac1 (Fig. 1C-E). The most strongly upregulated transcripts included characterized UPR^{ER} targets *KAR2, ULI1, PDI1,* and *ERO1* [Fig. 1C-E; (Chapman et al., 1998; Metzger and Michaelis, 2008)]. When we evaluated translation levels (based on ribosome footprint density), we saw prominent

Author Manuscript Author Manuscript Author Manuscript Author Manuscript

induction of the best-characterized Hac1 targets, as expected (Fig. S1A-E). Overall, we identified 477 genes as showing a UPR^{ER}- and Hac1-dependent increase in translation of greater than 2-fold in this dataset. Genes in this group were strongly enriched for ER-localization and function, as expected (p-value for ER=2.64E-14; posttranslational protein targeting to membrane, translocation=1.33E-6; protein glycosylation=1.58E-5; note that this set is based on analysis of DTT data, but Tm treatment yields similar results; Table S1, S2, Fig. S1A-D).

Normalizing translation levels to mRNA levels allowed us to determine TEs across all annotated ORFs (Ingolia et al., 2009), enabling detection of Hac1-dependent TE shifts upon UPR^{ER} activation. Although UPR^{ER} activation has been reported to influence TEs of some genes (Krishnan et al., 2014; Labunskyy et al., 2014; Payne et al., 2008), little is known about the pervasiveness of or potential mechanisms behind such regulation. Rather, the UPR^{ER} has been defined primarily as a transcriptional response. Our data are consistent with this general model, with a clear cohort of UPR^{ER}-driven, Hac1-dependent up-regulated transcripts seen (Fig. 1C-E). However, evidence for several dozen translationally regulated genes also emerged from our data. As expected, *HAC1* was one of the most strongly translationally up-regulated genes upon DTT or Tm treatment (Fig. 1F, 1G). An additional small subset of annotated Hac1 transcriptional targets seemed to show translational up-regulation with UPR^{ER} activation, although the mechanistic basis for this remains unclear. The most prominent example was functionally uncharacterized ER-related gene *ULI1* (Metzger and Michaelis, 2008), which was also one of the most highly induced transcriptional targets of Hac1 (Fig. 1E). The large increase in *ULI1* TE seen upon DTT treatment may point to a new translational mechanism linked to UPR^{ER} activation (Fig. 1F-1H).

Additionally, several annotated Hac1 targets appeared to show a Hac1-dependent decrease in TE upon UPR^{ER} activation (Fig. 1F-H). This type of TF-dependent TE drop is a hallmark of LUTI-based regulation during meiotic differentiation (Cheng et al., 2018). Because transcription of poorly-translated LUTI mRNAs decreases production of canonical well-translated transcript isoforms, TF-driven LUTI mRNA synthesis is detected in ribosome profiling datasets as translational repression (Cheng et al., 2018). We focused our attention on investigating *HNT1*, an annotated Hac1 target that consistently showed strong Hac1-and UPR^{ER}-dependent translational repression [Fig. 1F-H; (Travers et al., 2000)], by comparing its regulation to that of the most well characterized Hac1 target, *KAR2*.

HNT1 is a conserved member of the histidine triad superfamily (Séraphin, 1992). Its cellular function remains unclear, although a mammalian family member has recently been implicated in regulation of m^7G mRNA caps, suggesting that this gene family may be involved in translation (Kiss et al., 2017a, 2017b). Before investigating *HNT1* regulation, we first confirmed that our dataset reported the expected mRNA induction of canonical UPR^{ER} targets. As expected, a single *KAR2* mRNA isoform accumulated in a UPR^{ER}- and Hac1-dependent manner, as judged by northern blotting (Fig. 2A, S2A). *KAR2* mRNA was well-translated when present, with little change in TE seen upon UPR^{ER} activation (Fig. 2B). In contrast, while UPR^{ER} activation resulted in increased overall *HNT1* mRNA levels (Fig. S3B), it also resulted in a shift in the transcript isoforms present in cells. A longer *HNT1*

Author Manuscript Author Manuscript Author Manuscript Author Manuscript

mRNA species was observed by mRNA-seq and northern blotting following 1 hr of DTT or Tm treatment (Fig. 2C, 2D, S2B, S3C). The presence of the longer transcript was associated with lower TE values for the *HNT1* ORF and with translation of at least three uORFs in its extended 5' leader (Fig. 2E, 2F). Despite exhibiting hallmarks of LUTI-based regulation, the canonical *HNT1* transcript persisted after 1 hr of UPR^{ER} induction (Fig. 2D, S2B, S3C). Because the first LUTI case defined, $NDC80^{LUTI}$, resulted in complete disappearance of the canonical *NDC80* transcript when induced, we wondered if the apparently weaker LUTI induction observed for *HNT1* during the UPR^{ER} would be sufficient to have an effect on Hnt1 protein levels. We epitope-tagged endogenous Hnt1 and performed western blotting to detect protein levels following UPR^{ER} induction. Within 2 hr of DTT or Tm treatment, Hnt1 levels dropped to less than 50% of their levels prior to drug treatment (Fig. 2I-J). We confirmed that, like canonical UPR target *KAR2* (Fig. S3A), production of the long *HNT1* transcript isoform was dependent on *IRE1*, and thus part of the canonical UPR^{ER} (Fig. S3C).

We identified a strong type-2 UPR-responsive element (UPRE2), a DNA motif associated with Hac1 biding in the promoters of some UPR^{ER} targets (Patil et al., 2004), close to the distal *HNT1* TSS (Fig. 2C). The location of the UPRE2, coupled with the observation that induction of the longer transcript was dependent on *HAC1*, led us to hypothesize that the long *HNT1* isoform was a direct Hac1 target. To test this hypothesis, we constructed reporters containing *GFP* under control of the extended promoter region of *HNT1*, either with an intact UPRE2 adjacent to the distal TSS or a mutated motif (Fig. 2K). Following 90 min of DTT treatment, cells harboring *pHNT1-GFP* produced a high level of an extended *GFP* transcript isoform whose expression was severely reduced in the *pHNT1ΔUPRE2-GFP* mutant (Figure 2L, S2C, S3D). GFP protein levels in the WT reporter, but not the UPRE2 mutant, mirrored those of Hnt1 following UPR^{ER} induction (Fig. 2M, 2N). We concluded that *HNT1* is a LUTI target of Hac1 and that the UPR^{ER} involves coordinated activation and repression of target gene expression through Hac1-regulated alternate TSS usage. We suspected that *HNT1* might be just one of a class of "negative" targets of Hac1 and thus performed a systematic analysis of our data, searching for the expected signatures of Hac1 LUTI targets, including Hac1-dependent decreases in TE and appearances of 5' extended transcripts (Cheng et al., 2018). We identified 18 additional potential LUTI targets (Table 1).

A degradable version of Hac1 enables high-confidence identification of its targets

Confidently identifying Hac1-dependent targets of the UPR^{ER}, whether canonical (positive) or non-canonical (LUTI-based negative), was done here and previously by using comparison of WT cells to those deleted for *HAC1* or other core UPR^{ER} genes (Travers et al., 2000). While this has been a valuable approach, the risk in comparing gene expression measurements from WT cells and constitutive mutants is that it is difficult to ensure that secondary effects—on gene expression and in the form of genetic suppressors—are not confounding, resulting in misinterpretation of results. Such suppressors have been reported in *hac1Δ* cells, including in our strain background (Lee et al., 2003). We were concerned that perhaps our identification of non-canonical Hac1 targets might be an unexpected artifact of such secondary effects. We therefore replaced Hac1 with a version that contained an auxininducible degron (AID) tag and thus could be depleted on-demand by auxin addition. We found that AID-Hac1 rescued the growth defect of *hac1Δ* cells grown with DTT,

Author Manuscript Author Manuscript Author Manuscript Author Manuscript

suggesting normal functionality [Fig. 3A, 3B;(Nishimura et al., 2009)]. AID-Hac1 was stable in the presence of auxin in strains lacking the exogenous plant *TIR1* F-box auxin receptor gene, but in strains carrying *TIR1*, AID-Hac1 that accumulated during DTT pre-treatment was rapidly depleted upon auxin addition (Fig. 3C, 3D). Notably, AID-Hac1 protein was efficiently, but not fully, depleted in this background. As a result, we expected gene expression effects measured by comparing *AID-HAC1 TIR1* cells with and without auxin to be dampened relative to those from comparison of WT and *hac1Δ* cells.

Given that auxin-mediated degradation should be cytoplasmic, we were concerned that a persisting nuclear pool of AID-Hac1 may be capable of robustly carrying out its TF function, spatially isolated from the location of degradation. To investigate this, we analyzed expression of *KAR2* in cells that were treated with auxin following 45 min DTT pre-treatment. *KAR2* levels were rapidly reduced under these conditions, suggesting that auxin-induced Hac1 degradation reduced its TF activity (Fig. 3E, S2D). This result indicated that kinetic experiments using *AID-HAC1* cells might allow confident prediction of direct Hac1 transcriptional targets. The long isoform of *HNT1* (*HNT1*^{LUTI}) showed similar dynamics to the *KAR2* transcript, declining to undetectable levels within 20 min of auxin treatment following DTT pre-treatment (Fig. 3F, S2E). This rapid timing provided additional evidence that the *HNT1*^{LUTI} is a direct target of Hac1.

Although robust changes to transcription were observed by this strategy, effects on protein level of the canonical target Kar2 were not readily reversible upon auxin addition (data not shown), perhaps because Kar2 protein is not rapidly turned over under these circumstances. Because we have found assaying protein level to be useful in determining whether a given transcriptional target is positive or negative (Cheng et al., 2018), we reasoned that pre-treating cells with auxin and subsequently inducing the UPR^{ER} would be a more fruitful strategy. To this end, we pre-treated cells with auxin for 15 min and then added DTT for up to 2 hr. In cells lacking *TIR1, KAR2* mRNA and protein levels revealed the expected induction upon DTT treatment regardless of auxin addition (Fig. 3G-I, S2F). In contrast, in the *TIR1* background, DTT-dependent increases in *KAR2* transcript and protein levels were only observed if cells were pre-treated with vehicle. When pre-treated with auxin (depleting Hac1), efficient *KAR2* induction was largely prevented (Fig. 3G-I, S2F).

We next performed a new set of global gene expression measurements using the *AID-HAC1* strain background (Fig. 4A). We again measured mRNA and translation levels, and additionally collected matched extract for mass spectrometry in order to more completely evaluate Hac1-dependent effects on cellular physiology during the UPR^{ER}. Global effects on mRNA and translation were similar to those observed in our previous WT/*hac1Δ* experiment (Fig. 4B, 4C, Fig. S4), but as expected, were milder than observed when comparing WT and *hac1Δ* cells. Nevertheless, we observed UPR^{ER}- and Hac1-dependent activation of known Hac1 targets, including *KAR2, ERO1,* and *PDI1* (Fig. 4B, S4). DTT-dependent induction of *HNT1*^{LUTI} was observed by mRNA-seq, but not in cells depleted of Hac1 (Fig. 4D). As before, translation of *HNT1* was decreased in a UPR^{ER} and Hac1-dependent manner and was associated with translation of uORFs in the extended 5’ leader, unless cells were depleted of Hac1 (Fig. 4C, 4E, 4F, S4E-G). We confirmed the DTT and Hac1-dependent induction of *HNT1*^{LUTI}, as well as the correlated decrease in Hnt1 protein level, by northern

Author Manuscript Author Manuscript Author Manuscript Author Manuscript

and western blotting (Fig. 4G-4I, S2G). We concluded that expression of *HNT1*^{LUTI} results in decreased Hnt1 protein levels, dependent on Hac1, suggesting that our original results were not an artifact of constitutive *HAC1* deletion (Fig. 2).

Hac1 "negative" targets include genes involved in ETC function

We found that 15 of the original 19 annotated long transcript isoforms could be confirmed as UPR^{ER}- and Hac1-dependent in the *AID-HAC1* background (Table 1). Of the four that could not, two did not show the expected TE decrease and two showed the decrease independent of Hac1. These cases may be a result of yet undefined secondary effects in the delete background. We concluded that a set of LUTI targets is induced by Hac1 as part of the UPR^{ER}.

Several of the 15 Hac1-dependent LUTI-regulated genes were involved in electron transport chain (ETC) function, specifically in assembly of Complex IV (cytochrome c oxidase), which LUTI targets *COX20, OXA1,* and *SOM1* all contribute to. We thus investigated the possibility that down-regulation of ETC components might be linked to UPR^{ER} activation and partly controlled by LUTI-based regulation. We first examined the regulation of *COX20*, a gene responsible for Cox2 processing and subsequent assembly of Complex IV (Hell et al., 2000). We confirmed the Hac1-dependent appearance of a dramatically 5' extended transcript isoform upon UPR^{ER} activation by mRNA-seq (Fig. 5A) and translation of a uORF near the 5' end of this extended transcript, which was adjacent to a high-scoring UPRE2 (Fig. S5B). Northern blotting for *COX20* revealed Hac1-dependent induction of a longer transcript upon DTT or Tm treatment, confirming that the mRNA-seq data did not simply reflect a partially overlapping transcript that excluded the *COX20* ORF (Fig. 5B, 5C, S2H, S2I, S5A). This longer *COX20* transcript isoform was also dependent on *IRE1* (Fig. S5D).

We were initially concerned that the bands representing the two *COX20* transcript isoforms did not show the stoichiometry expected based on our mRNA-seq data from either large-scale experiment, with the longer transcript reproducibly resulting in a much fainter band than the canonical transcript. We attribute this effect to the large size difference between the transcripts (0.8 Kb vs approximately 2.6 Kb; Fig. 5A, S7K), as we observe that longer transcripts transfer less efficiently than shorter transcripts using our northern blotting protocol. Nevertheless, like the canonical UPR^{ER} target *KAR2*, production of *COX20*^{LUTI} was abrogated with Hac1 depletion after 45 min UPR^{ER} pre-activation, suggesting direct dependency on Hac1 (Fig. 5B, S2H). Upon UPR^{ER} activation, we observed a decrease in *COX20* TE and Cox20-3V5 protein that was alleviated when Hac1 was depleted (Figure 5E, 5F, S5C). This Cox20 protein decline was even more apparent in DTT-treated WT cells (Fig. 5G, 5H), and was similar in extent but delayed in timing upon Tm treatment, consistent with the slower appearance of *COX20*^{LUTI} upon Tm treatment (Fig. 5C, 5I, 5J, S2I, S5D). Importantly, levels of canonical target protein Kar2 continued to increase with Tm treatment over this timescale (Fig. S5E). Also consistently, the *COX20* TE decreased more dramatically with DTT treatment than with Tm treatment (Fig. 5D). We concluded that *COX20* is a LUTI target of Hac1, with protein levels that are down-regulated as part of the UPR^{ER}.

Author Manuscript Author Manuscript Author Manuscript Author Manuscript

UPR ^{ER}-activation drives a global proteomic and metabolic shift

Why do UPR^{ER}-activated cells couple up-regulation of canonical targets, like *KAR2*, with down-regulation of non-canonical ones, like *COX20*? In the case of *COX20*, the down-regulation of its protein level was intriguing, given its role in ETC function. The UPR^{ER} in flies has been associated with induction of glycolytic enzymes and a cell-type specific metabolic shift to increased glycolytic flux (Lee et al., 2015). A similar shift from aerobic respiration to glycolysis is commonly observed in cancer cells and termed the "Warburg effect" in that context (Warburg, 1956). We sought to determine whether such an effect might be a core part of the Hac1-dependent UPR^{ER} by using additional global measurements in our *AID-HAC1* system. First, we performed metabolomic profiling, comparing cells with and without UPR^{ER} activation by Tm, and with and without Hac1 depletion. Of all glycolysis and TCA intermediates measured, most did not change in a statistically significant manner in our experiment. Several did, however, and we noted that the two TCA intermediates (citrate and malate) that changed significantly between Hac1-containing and – depleted cells were lower in Tm-treated cells containing Hac1 than with its levels depleted, potentially suggesting reduced respiration in Hac1-containing UPR^{ER}-activated cells (Fig. S6A). Glycolysis-associated metabolites tended to either remain roughly constant or to be higher in UPR^{ER}-activated cells containing Hac1 (Fig. S6A). These results were subtle and, while consistent with a shift from respiration in Hac1-containing UPR^{ER}-activated cells, did not provide definitive proof due to our inability to detect statistically significant shifts in many relevant intermediates with and without *TIR1*. We hypothesized that this may have resulted from the dampened range of effects that we note above in Hac1-depletion experiments compared to those using WT vs. *hac1Δ* cells. Indeed, similar analyses in cells carrying *HAC1* showed consistent, significant dis-enrichment of TCA intermediates and enrichment of glycolytic intermediates with Tm treatment (Fig. 6A).

To more comprehensively determine the degree to which UPR^{ER} activation may couple down-regulation of specific physiological cellular processes—such as aerobic respiration—to up-regulation of classic UPR^{ER} targets like ER chaperones, we performed proteomic measurements in samples identical to those measured for mRNA and translation (Fig. 4A–4C, S4). We used TMT-based isobaric labeling to compare shifts in proteome composition with and without Hac1 depletion, and with and without UPR^{ER} activation. This experiment yielded a deep dataset, allowing comparison of the levels of 2577 proteins with and without DTT and Hac1 (Fig. 6B). The data were of high quality, revealing the expected patterns for Hntl, Cox20, and canonical UPR^{ER} targets (Fig. S6B). A broad view of the data revealed dramatic overall shifts in proteome composition with DTT addition, with a subset of these changes dependent on Hac1. A discrete cluster of 72 proteins, which included canonical targets Kar2, Ero1 Pdi1, and Lhs1, emerged as increased in a UPR^{ER}- and Hac1-dependent manner. GO analysis of the genes encoding these proteins (Fig. 6B; Table S3) showed that they were strongly enriched for roles in protein transport and ER function. A second cluster of l97 proteins showed increased protein expression following UPR^{ER} activation that was delayed following Hac1 depletion. GO analysis of the genes encoding them revealed strong enrichment for proteolysis functions and the ER-associated degradation (ERAD) pathway [Fig. 6B,Table S4; consistent with (Travers et al., 2000)]. A third cluster of 282 proteins showed decreased protein levels with UPR^{ER} activation, with at least partial dependence on

Author Manuscript Author Manuscript Author Manuscript Author Manuscript

Hac1. The associated genes were heavily enriched for roles in translation and ribosome assembly (Fig. 6B, Table S5). This observation is interesting, as the down- regulation of translation is a well-defined aspect of the UPR^{ER} in higher eukaryotes (Walter and Ron, 2011). This effect has thus far been less clear in budding yeast studies, and our results suggest that it warrants revisiting. Most interestingly, given the Hac1-dependent LUTI regulation seen for Cox20 and our hypothesis that metabolism shifts away from respiration in UPR^{ER}-activated cells, the genes encoding the group of UPR^{ER}-dependent down-regulated proteins was also enriched for roles in ATP synthesis coupled electron transport, oxidative phosphorylation, the ETC, cytochrome complexes, and the mitochondrial respiratory chain (Table S5). KEGG pathway analysis also revealed enrichment for components of the ETC and aerobic respiration (p=0.0027) among these down-regulated genes, further supporting a metabolic shift away from aerobic respiration as part of the UPR^{ER}. Finally, isolation of data for glycolytic enzymes revealed a complementary up-regulation of protein levels that was dependent on UPR^{ER} activation, although only some of these increases were dependent on Hac1 (Fig. S6C).

Because TMT-based measurements often yield values that appear dampened in range relative to other methods (Wenger et al., 2011), we also used label free quantification (LFQ), an orthogonal approach, on the same samples. This allowed for better determination of the degree of specific protein level changes following UPR^{ER} activation. LFQ analysis revealed trends that mirrored those seen with TMT-based quantification, but that were less muted in degree (Fig. S6B, S6D). As expected, UPR^{ER} induction still showed increased levels of canonical UPR^{ER} target proteins, such as Kar2 (Fig. 6C). Untagged Hnt1 protein levels were dramatically reduced in a Hac1-dependent manner, to an even greater degree than observed for the epitope-tagged protein. The degree of Hnt1 decrease in Hac1-containing cells relative to cells depleted for Hac1 was roughly equivalent to the degree of Kar2 increase (Fig. S6D), suggesting potential for a strong cellular effect from the Hac1-dependent induction of $HNT1^{LUTI}$. Cox20 showed a 2.4-fold decrease in UPR^{ER}-activated cells containing Hac1 compared to those depleted for it (Fig. S6D), which was similar to the decrease observed for the epitope-tagged protein (Fig. 5G-J) and which suggests potential for a strong physiological effect.

Preventing aerobic respiration ameliorates cellular growth defects due to UPR^{ER} activation

Oxygen consumption assays revealed a time-dependent, significant decrease in oxygen consumption rates (OCR) of cells treated with Tm (Fig. 6D), consistent with a decrease in aerobic respiration in UPR^{ER}-activated cells. To investigate a potential functional role for down-regulated aerobic respiration in the UPR^{ER}, we leveraged the fact that budding yeast cells can grow well in rich media in the absence of aerobic respiration resulting from mutation in ETC-related genes. We examined cells deleted for *PET100*, a gene that is required for assembly of ETC complex IV (Church et al., 1996). We compared cell doubling of untreated WT and *pet100Δ* cells in rich media, observing the expected moderate growth defect in the latter background (Fig. 6E). We then repeated the experiment in the presence of DTT and observed that, while both WT and *pet100Δ* cells doubled more slowly than in untreated conditions, the previously observed growth defect in *pet100Δ* cells relative to WT was strongly suppressed (Fig. 6F). In fact, under these conditions, *pet100Δ* cells robustly

Author Manuscript Author Manuscript Author Manuscript Author Manuscript

surpassed WT cells in their growth rate. Because of possible confounding effects of using a strong reducing agent like DTT for these experiments, we performed a similar analysis instead activating the UPR^{ER} by Tm addition, which is stable enough for use in plate-based growth assays, in contrast to DTT. Cell growth following dilution on plates containing 0 to 0.75μg/mL Tm produced results similar to the DTT growth rate data (Fig. 6G). WT cells formed larger colonies than *pet100Δ* cells without Tm, but with increasing Tm concentration, *pet100Δ* cells were able to surpass WT in growth ability. Based on these experiments, we concluded that down-regulation of factors responsible for aerobic respiration, which accompanies UPR^{ER} activation and is partially modulated by Hac1 activity, is likely to be a functionally important component of the UPR^{ER} in yeast.

Discussion:

Here we report that, in addition to its characterized role in the induction of ER-related target genes during the UPR^{ER}, Hac1 also down-regulates a set of genes by driving production of mRNAs that ultimately result in reduced protein levels. Hac1 thus coordinates up- and down-regulation of distinct targets, contributing to a shift in the proteome and metabolism of UPR^{ER}-activated cells (Fig. 6H). We report that Hac1-dependent transcription results in down-regulation of at least 15 genes during the UPR^{ER} (Table 1). More broadly, our study provides a set of new examples of LUTI-based regulation, a recently defined mode of gene regulatory control that pervasively shapes the proteome of budding yeast cells during the meiotic program (Cheng et al., 2018; Tresenrider and Ünal, 2017). The fact that this regulation can be mediated by the conserved transcription factor Hac1 as part of a conserved stress response suggests that it may be broadly used in transcriptional regulatory responses.

A key component of LUTI-based regulation is cis-silencing of the proximal TSS (Chia et al., 2017). While transcriptional interference is well established [for example (Cullen et al., 1984; Martens et al., 2004)], LUTI-based regulation involves production of an interfering transcript containing a coding region that is translationally repressed. The ultimate effect of this regulation is counterintuitive from a classical gene regulatory perspective, as it involves mRNA-inducing TFs acting effectively as repressors of gene expression and results in an uncoupling of overall mRNA and protein synthesis levels due to a greater importance of the isoform *type* than overall transcript levels in directing protein synthesis (Chen et al., 2017; Cheng et al., 2018). This can be seen in the Hac1 LUTI cases defined here, including *HNT1*, which was previously reported to be an up-regulated UPR^{ER} target based on Hac1-dependent mRNA accumulation in response to UPR^{ER} activation (Travers et al., 2000). Consistently, we find that the total mRNA abundance for *HNT1* is increased during the UPR^{ER}, dependent on Hac1. However, expression of the Hac1-dependent LUTI transcript that accounts for this mRNA increase results in *decreased* protein production. Due to their relative ease of measurement, mRNA abundance values have been widely used as a proxy for gene expression output. While these measurements are undoubtedly useful and may accurately predict protein level changes in many instances, they can also be misleading. *HNT1* is a prime example of this in the simple and well-defined cellular response explored here. It is likely that many other existing gene expression datasets hold such examples, which may lead to misinterpretation of the cellular consequences of transcriptional responses.

Author Manuscript Author Manuscript Author Manuscript Author Manuscript

While cases like *HNT1* are particularly striking, an overall mRNA increase is not necessarily seen in cases of LUTI production. Most of the new cases identified here instead exhibit a shift in type of mRNA made without dramatically altering total mRNA quantity for a given gene. In these cases, mRNA levels are uninformative unless this information is integrated with translation data, and ideally measurements of protein, the ultimate gene expression output. Our use of integrated measurements from matched extract enabled a view of the UPR^{ER} gene expression program that would have been impossible to gain from analysis of existing gene expression datasets. For example, matched protein measurements in our study were key to showing that this unconventional mechanism has a cellular effect. Our protein data, which shows decreases in levels of LUTI-regulated proteins within 1-2 hr of UPR^{ER} activation, argue that active degradation of existing protein pools is likely also occurring under our experimental conditions, although we do not yet know the mechanism for the proteins explored here. Similarly, for this mechanism to be effective, transcript half-lives must be relatively short. While transcript destabilization is actively achieved during periods of UPR^{ER} activation for a subset of ER-localized mRNAs by regulated Ire1-dependent decay (RIDD) in some organisms [(Hollien et al., 2009); reviewed in (Maurel et al., 2014)], this mechanism has not been observed in budding yeast. A recent study, however, reports mRNA half-lives in budding yeast to be much shorter than previously thought (Chan et al., 2017), suggesting that an additional mechanism for degradation of canonical transcripts of LUTI-regulated genes may not be required for this regulation to be rapid and effective.

Our study is not the first to suggest that the UPR^{ER} may directly or indirectly result in translational down-regulation of a set of genes. Several studies have investigated this possibility and reanalysis of their data, in light of our LUTI model and complementary measurements, reveals results consistent with our findings. For example, microarray analyses of polysome fractions with and without DTT treatment showed that ribosome biogenesis genes were translationally repressed in a DTT-dependent manner, while canonical targets, like *ERO1*, were well-translated under these conditions (Payne et al., 2008). Interestingly, 10 of the 15 Hac1 LUTI targets that we annotate here—including *HNT1* and *COX20*—were among the genes detected in that study to show a DTT-dependent shift from polysomes to a subpolysome fraction, indicating translational repression (Table 1). More recently, mRNA-seq and ribosome profiling was reported from cells with and without Tm treatment (Labunskyy et al., 2014). This study concluded that genes that were up-regulated in response to Tm-driven UPR^{ER} activation tended to be transcriptional targets of Hac1 and that down-regulated targets tended to be regulated at the level of TE (Labunskyy et al., 2014). This is consistent with our finding that Hac1 acts as a transcriptional activator for canonical targets and indirectly acts as a translational repressor for LUTI targets. Intriguingly, the Tm-dependent translationally down- regulated genes in this previous ribosome profiling study were enriched for roles in ATP metabolic processes ($p=0.026$) and mitochondria ($p=0.030$), and several ETC-related genes were in this set, including two that are required for Complex IV assembly [Table S6; (Labunskyy et al., 2014)]. Although their results are consistent with our data, neither of these previous studies included strains deleted or depleted for *HAC1*, so the degree to which effects were dependent on Hac1 was unclear, and the lack of transcript isoform data available precludes reanalysis for other features of LUTI-based regulation.

Author Manuscript Author Manuscript Author Manuscript Author Manuscript

Our study reveals two separate but linked key findings: the existence of Hac1- dependent LUTI-based regulation and coordinated up- and down-shifting of levels of distinct protein groups during the UPR^{ER}. We propose, based on examples like *COX20* that the down-regulation of genes involved in aerobic respiration observed during the UPR^{ER} is at least partially mediated by Hac1-based induction of repressive mRNA isoforms. However, we do not find evidence that all respiratory protein down-regulation is dependent on this mechanism. For most of the ETC proteins that we measured to be reduced during UPR^{ER} activation, no associated alternate transcript isoforms were observed. This could be a result of the challenges in predicting alternate transcript isoforms based on mRNA-seq data alone, as we did in this study as a necessity, but it seems unlikely that LUTI-based regulation can directly explain the down-regulation of all proteins observed here to decrease during the UPR^{ER}. It is more likely that either a few LUTI-regulated genes act as linchpin components that cause remaining complex members to become unstable or that there are parallel, potentially synergistic mechanisms to decrease levels of respiratory proteins during the UPR^{ER}. The cellular consequence of our newly identified cases of Hac1-dependent, LUTI-based gene repression is another outstanding question. We note an apparent enrichment for ETC function among the group, but we have not identified enough cases to confidently assay statistical significance for LUTI-based regulation for this or other processes. It is likely, however, that ETC regulation is not the function of all newly proposed Hac1 LUTI mRNAs. Although several of the 15 genes encode mitochondrial proteins, most do not. Additionally, some of these genes, including *HNT1*, have such poorly defined cellular roles that determining the possible importance of their down-regulation during the UPR^{ER} is difficult at this time.

Our proteomic data suggest a reallocation of cellular resources in UPR^{ER}-activated cells from ribosome biogenesis to ER function, and away from respiration. It is not surprising that a stress response would require a shift in proteome content, but in this case, it is unclear why the Warburg-like shift in ATP-generation mode would bolster cellular fitness during the UPR^{ER} [Fig. 6;(Lee et al., 2015)]. Nonetheless, our results show that such a shift occurs and is advantageous, as cells without the ability to respire show a growth advantage relative to WT cells when grown in UPR^{ER}- activating conditions. While this result suggests that this shift is a relevant functional component of the UPR^{ER}, it does not explain *why* this is the case. It has been proposed that reduction of TCA cycle activity associated with the Warburg effect seen in cancer cells allows acetyl-CoA to be shunted towards the robust new lipid synthesis required for membrane expansion that accompanies rapid cell division (Vander Heiden et al., 2009). A similar explanation is enticing in this case, as one of the hallmarks of UPR^{ER} activation is an increase in ER membrane volume, which requires new lipid synthesis and membrane expansion. It is alternatively possible that it is important to down-regulate an alternate ETC function for the UPR^{ER}. For example, it has recently been shown that the redox function of the ETC through NAD+ recycling is responsible for the growth defect seen in ETC-deficient mammalian cells (Titov et al., 2016).

Why do UPR^{ER} -activated cells employ the LUTI mechanism for down-regulation of a subset of targets? In principle, a transcriptional repressor that is linked to UPR^{ER} activation should allow a similar overall effect, although no such regulator has been identified, to our knowledge. We argue, however, that LUTI-based regulation is as effective as this alternative

Author Manuscript Author Manuscript Author Manuscript Author Manuscript

classical mode of regulation. We note that several Hac1- dependent LUTI target proteins, including Cox20 and Som1, show robust *up- regulation* in response to DTT in the absence of Hac1. Hac1-dependent induction of the LUTI transcript in these cases appears effective at preventing and even reversing these protein level increases. Further, this modular mechanism of regulation allows cells to use pre-existing trans-factors for both up- and down-regulation of targets, precluding the need for an additional protein to act as a dedicated transcriptional repressor (Chen et al., 2017; Cheng et al., 2018). Perhaps most importantly, a major advantage of this mechanism is that the use of a single TF—Hac1 in this case—allows for direct coordination of up-regulation of some genes with down-regulation of others (Cheng et al., 2018). This type of coordination is an attractive strategy for mediating rapid cellular responses to acute stress. The fact that a well-studied, conserved stress response program employs this unconventional mode of gene regulation suggests that LUTI-based regulation may be broadly used to modulate gene expression in contexts of cellular state change. Construction of new, integrated datasets aimed at identifying such regulation, along with revisiting traditional conceptual models of gene expression, will be required to ultimately determine whether this is the case.

STAR Methods

CONTACT FOR REAGENT AND RESOURCE SHARING

Further information and requests for resources and reagents should be directed to and will be fulfilled by the Lead Contact, Gloria Brar (gabrar@berkeley.edu).

EXPERIMENTAL MODEL AND SUBJECT DETAILS

Yeast strain construction

All experiments were performed using *Saccharomyces cerevisiae* strains of the SK1 background.

Gene deletion strains: Deletions were created by one-step gene deletion, as described in (Longtine et al., 1998).

AID-HAC1 strain: Construction of this strain required deleting endogenous *HAC1* and replacing it ectopically with an auxin-inducible degron (AID)-tagged version. We ensured that the promoter, intron, and UTRs, which are all required for proper regulation of *HAC1*, were not disrupted in this construct [Fig. 3A; (Aragón et al., 2009; Bowring and Llewellyn, 2001; Ogawa and Mori, 2004; Sathe et al., 2015)]. To build the allele, we cloned 507bp upstream of the *HAC1* ORF in front of a 3V5 tag, followed by the IAA7 degron, the *HAC1* ORF, and 844bp downstream of the *HAC1* stop codon. The entire construct was cloned into a *LEU2* integrating vector (resulting in plasmid pÜB1073) and the AflII (NEB) digestion product was subsequently transformed into a strain heterozygous for *hac1Δ*. Following sporulation, haploids were chosen that carried the *AID-HAC1* allele as their sole source of Hac1.

Author Manuscript Author Manuscript Author Manuscript Author Manuscript

HNT1-3V5 and COX20-3V5 strains: A c-terminal *3V5* tag, marked by a G418 resistance cassette, was integrated into the endogenous locus, replacing the stop codon.

GFP reporter strains: For *pHNT1-GFP, pHNT1* (−600 to +42) was cloned ahead of a ubiquitin-GFP fusion, followed by the *Candida albicans ADH1* terminator, resulting in pÜB1397. For *pHNTΔUPRE2-GFP*, the first five of the six bp in the UPRE2 motif starting at −284 were deleted from pÜB1397 via Q5 mutagenesis, resulting in pÜB1406. Constructs were integrated at the *TRP1* locus via transformation with the PmeI (NEB) digestion product of the relevant plasmid.

Yeast growth conditions

Strains were grown in YEPD(2%) at 30C, with shaking. Plate-based growth assays were carried out on YEPD(4%) plates at 30C.

METHOD DETAILS

Sample collection for sequencing experiments

WT/ hac1Δ: BrÜn 1362 (WT) and 4431(hac1Δ) were inoculated into YEPD and grown at 30C overnight, then diluted to OD_{600}0.05 in YEPD. After approximately 2 doublings, cultures were split into 3 subcultures. Per strain, a first subculture received no treatment, a second was treated with 5mM DTT, and a third was treated with 2μg/mL Tm (Calbiochem). After 1 hr, 500 mL samples were collected as in (Brar et al., 2012), using 30 sec cycloheximide treatment, filtration, and flash freezing (in 2 portions - ~90% for ribosome profiling and ~10% for mRNA-sequencing). 2mL flash frozen buffer (20mM TRIS pH8, 140mM KCl, 1.5mM $MgCl_2$, 100μg/mL cycloheximide, 1% Triton X-100) was added to each ribosome profiling aliquot. Samples were lysed via Retsch mixermilling (6X 3 min, 15 Hz). Resulting powder was thawed and spun at 4C for 5 min, 3,000 × g. Supernatant was removed and cleared at 4C for 10 min, 20,000 × g.

AID-HAC1: BrÜn 10532 (*AID-HAC1 -TIR1*) and 10744(*AID-HAC1 +TIR1*) were inoculated into YEPD and grown at 30C overnight, then diluted to OD_{600}0.05 in YEPD. After approximately 2 doublings, cultures were split into 2 subcultures. Per strain, one subculture was treated with 500μM auxin (Sigma) and 4μM IP_6 (Sigma) and the other with equivalent volumes of DMSO and water. After 15 min, the subcultures treated with auxin and IP6 were further split into 2 subcultures. Per strain, 1 auxin-pre-treated culture was not treated further (+auxin), and 1 was treated with 5mM DTT (+auxin +DTT). For each strain, the DMSO pre-treated subculture was treated with 5mM DTT (+DTT +vehicle). After 1 hr, 500 mL per culture was harvested identically as in the WT/*hac1Δ* experiment, except the buffer was supplemented with 2μg/mL Aprotinin (Sigma), 10μg/mL Leupeptin (Sigma), 1 mM PMSF (Sigma), 1:100 PIC2 (Sigma), and 1:100 PIC3 (Sigma). After 1 additional hr, a second 500 mL sample was harvested from each culture. Extract was prepared as in the WT/*hac1Δ* experiment, and identical extract was used for ribosome profiling and mass spectrometry.

Author Manuscript Author Manuscript Author Manuscript Author Manuscript

Additional sample collection for protein/RNA

WT/hac1Δ transcript comparisons: One biological replicate was derived from total RNA prepared for the sequencing experiment described above. An additional replicate was collected similarly, except was harvested by filtration without the addition of cycloheximide.

WT/ ire1Δ transcript comparisons: Two biological replicates were collected as follows. BrÜn 15 (WT) and 15924 (*ire1Δ*) were inoculated into YEPD and grown at 30C overnight, then diluted to OD_{600}0.05 in YEPD. After approximately 2 doublings, cultures were split into 3 subcultures. Per strain, a first subculture received no treatment, a second was treated with 5mM DTT, and a third was treated with 2μg/mL Tm (Calbiochem). Samples were harvested at the indicated times by filtration.

Additional AID-HAC1 transcript comparisons: For cases where cells were pre-treated with auxin and subsequently treated with DTT, one biological replicate was derived from total RNA prepared for the sequencing experiment above. An additional replicate was collected similarly, except was directly harvested by filtration without the addition of cycloheximide. For analysis of AID-Hac1 protein levels in these experiments, 3 biological replicates were collected similarly except 2.5 OD units were harvested at each time point and treated with 5% trichloroacetic acid (TCA).

For cases where cells were pre-treated with DTT and subsequently treated with auxin, 2 biological replicates were collected as follows. BrÜn 10532 (*AID-HAC1 - TIR1*) and 10744(*AID-HAC1 +TIR1*) were inoculated into YEPD and grown at 30C overnight, then diluted to OD_{600}0.05 in YEPD. After approximately 2 doublings, the BrÜn 10744 culture was split into 2 subcultures. BrÜn 10532 and one of the BrÜn 10744 subcultures were treated with 5 mM DTT, while the other BrÜn 10744 subculture remained untreated. After 45 min, samples from each culture were collected by filtration. Both DTT-treated cultures were then treated with 500μM auxin (Sigma) and 4μM IP_6 (Sigma/Santa Cruz Biotechnology), while the untreated culture was treated with DMSO. Additional samples were collected by filtration at the indicated times. For analysis of Kar2 protein levels in these experiments, 3 biological replicates were collected similarly except 2.5 OD units were harvested at each time point and treated with 5% TCA.

Evaluation of HNT1 and COX20 expression: For evaluation of Hnt1 and Cox20 protein levels upon DTT or Tm treatment (Fig. 2G, 2I, 5G, 5I), BrÜn 10778 (*HNT1-3V5*) and 10781 (*COX20-3V5*) were harvested as follows. The appropriate strain was inoculated into YEPD and grown at 30C overnight, then diluted to OD_{600}0.05 in YEPD. After ~2 doublings, 2.5 OD units were collected and treated with 5% TCA, and cultures were subsequently treated with either DTT or Tm. Additional samples (2.5 OD units each time) were taken at the indicated times. Three full biological replicates were harvested for each condition. For similar experiments in the *AID-HAC1* background,BrÜn 10924 and 10925 were used for Hnt1 analysis, and BrÜn 10929 and 11133 were used for Cox20 analysis. Collection was the same, except that cultures were pre-treated for 15 min with 500μM auxin (Sigma) and 4μM IP_6 (Sigma) prior to initial sample collection and 5mM DTT treatment.

Author Manuscript Author Manuscript Author Manuscript Author Manuscript

Additionally, approximately 20mL per culture was collected at each time point and used for downstream RNA applications.

Evaluation of GFP reporter expression: For evaluation of *GFP* transcript levels, BrÜn 15968 (*pHNT1-GFP*) and 16374 (*pHNT1ΔUPRE2-GFP*) were inoculated into YEPD and grown at 30C overnight, then diluted to OD_{600}0.05 in YEPD. After ~2 doublings, cultures were treated with 5mM DTT. Following 90 min treatment, samples were harvested by filtration and flash-frozen for total RNA isolation. Two biological replicates were harvested for each condition.

For evaluation of GFP protein levels (Fig. 2M), BrÜn 15968 (*pHNT1-GFP*) and 16374 (*pHNT1ΔUPRE2-GFP*) were inoculated into YEPD and grown at 30C overnight, then diluted to OD_{600}0.05 in YEPD. After ~2 doublings, 2.5 OD units were collected and treated with 5% TCA, and cultures were subsequently treated with 5mM DTT. Additional samples (2.5 OD units each time) were taken at the indicated times. Three biological replicates were harvested for each condition.

Growth curves

For Fig. 3B, growth curve was performed as follows: BrÜn 13 (WT), BrÜn 4431 (*hac1Δ*), and BrÜn 10353 (*AID-HAC1*) were inoculated into YEPD and grown at 30C overnight, then diluted to OD_{600}0.05 in YEPD. After 7 hr, cultures were back-diluted to OD_{600}0.15 in YEPD. In a 96-well plate, 150μL cells were treated in triplicate with 2.5mM DTT. Cultures were grown overnight in a 30C, shaking plate reader (Tecan Infinite M1000), with absorbance at 600nm measurements taken every 15 min. Absorbance readings in Fig. 3B represent averaged values across triplicate wells.

For Fig. 6E-F, growth curves were performed as follows: BrÜn 15 (WT) and BrÜn 2781 (*pet100Δ*) were inoculated into YEPD and grown at 30C overnight, then diluted to OD_{600}0.05. After ~2 doublings, cultures were split into 2 subcultures, one of which remained untreated and one of which was treated with 5mM DTT. OD_{600} readings were taken every hr. OD600 values in Fig. 6E-F are normalized to the exact OD_{600} reading just before treatment and represent average fold change from starting OD_{600} across 3 biological replicates.

Plate-based growth assays

BrÜn 15 (WT) and BrÜn *2781(pet100Δ*) were inoculated into YEPD and grown at 30C overnight, then diluted to OD_{600}0.2 in YEPD. Approximately 4.5 hr later, cultures were diluted to OD_{600}0.1 in water. Samples were briefly sonicated to prevent clumping, and 5-fold dilutions were prepared in water. 3 μL of each dilution were plated on YEPD (4%) containing 0μg, 0.5μg or 0.75μg/mL Tm. Plates were imaged after 2 nights at 30C.

Northern blotting

All RNA was isolated using the hot acid phenol method. 8-10μg of total RNA was denatured in glyoxal mix [1M glyoxal (Sigma), 50% DMSO, 10mM $NaPO_4$ pH 6.8] for 10 min at 70C. Denatured samples were loaded onto a 1.1% agarose gel, separated at 116V for 3 hr, and

Author Manuscript Author Manuscript Author Manuscript Author Manuscript

transferred overnight to a nylon membrane [Hybond-N+ (GE)]. Following UV crosslinking and methylene blue staining, the membrane was blocked at 68C for at least 45 min with Ultrahyb buffer (Invitrogen) supplemented with boiled sonicated salmon sperm DNA (Agilent). All probe templates were generated by PCR (primers in Table S7) of WT yeast genomic DNA, except the *GFP* probe template, which was generated by amplification from a GFP-containing plasmid. The probe was in vitro transcribed [MaxiScript T7 Kit (Invitrogen)] using all kit components, except cold UTP was replaced with alpha-P32 labeled UTP (PerkinElmer). The blot was incubated with the hot probe at 68C overnight, and subsequently washed for 2X 5 min at RT with low stringency wash buffer (2X SSC, 0.1% SDS) and 2X 15 min at 68C with high stringency wash buffer (0.1X SSC, 0.1% SDS). Typhoon phosphor-imaging was used for visualization. For each transcript probed, at least 2 biological replicates were performed and sizing was confirmed on a sample blot with ladders (Fig. S7G-E) and, more routinely, by comparison to rRNA bands. In our experience, likely due to their highly stable structural features, rRNA (2.0 kB and 3.8 kB) species tend to migrate slightly faster than would be expected for mRNAs (for example, Fig. S7I-J), making all of our size comparisons approximate.

Western blotting

Western blotting was performed using a TCA protocol, similar to that described by (Chen et al., 2017). Briefly, 2.5 OD units of culture were treated with 5% TCA at 4C for at least 10 min. Samples were then washed with 1mL acetone. Acetone was aspirated and pellets were dried overnight at RT. Lysates were made by adding 100µl protein lysis buffer [50mM TE, 3mM DTT, 1.1mM PMSF (Sigma), 1µM pepstatin A, 1X protease inhibitor cocktail (Roche)] and 1 volume acid-washed glass beads (Sigma), and bead-beating for 5 min at RT. 3X SDS loading buffer was added and samples were boiled for 5 min. Beads were pelleted by centrifugation and 5µL supernatant was loaded onto 4-12% Bis-Tris polyacrylamide gels. Following electrophoresis, proteins were transferred using a semi-dry transfer apparatus (Trans-Blot Turbo, BioRad). The following antibodies were used: mouse anti-V5 (Invitrogen, 1:2,000), rat anti-tubulin (Serotec, 1:10,000), rabbit anti-Kar2 (gift of Mark Rose, 1:100,000), mouse anti-GFP (Clontech, 1:500), goat anti-rat680 (LI-COR, 1:15,000), goat anti-mouse800 (LI-COR, 1:15,000), goat anti-rabbit 800 (LI-COR, 1:15,000). Example uncropped blots for all proteins examined in this work are shown in Fig. S7 (L-P) to demonstrate sizing relative to ladder.

Ribosome profiling library generation

Ribosome profiling libraries were prepared as described as in (Cheng et al., 2018). Briefly, footprints were prepared by treating extract with 15U RNAse I (Ambion) per A_{260} unit for 1 hr at RT. Monosomes were isolated by sucrose gradient (10-50%). RNA was isolated by the hot acid phenol method. Samples were size-selected (by PAGE), dephosphorylated [PNK (NEB)], polyA-tailed [PolyA polymerase (NEB) with oCJ200-oligodT], subtracted of rRNA [MyOne Streptavidin C1 dynabeads (Invitrogen) with asDNA1b-3b], and reverse transcribed [Superscript III (Invitrogen)]. RT products were size-selected (by PAGE), circularized [Circ ligase (Epicenter)], and PCR amplified [Phusion polymerase (NEB) with oNTI231and index primers]. Following gel purification, libraries were sequenced using standard Illumina oligos.

Author Manuscript Author Manuscript Author Manuscript Author Manuscript

mRNA-sequencing library generation

mRNA-sequencing libraries were prepared as described in (Cheng et al., 2018). Briefly, RNA was extracted by the hot acid phenol method and was polyA-selected [oligodT Dynabeads (Ambion)]. Samples were alkaline fragmented, then size-selected (by PAGE) and subsequently dephosphorylated, polyA-tailed, and reverse transcribed as for the ribosome profiling libraries. RT products were similarly size-selected, circularized, and PCR amplified. Following gel purification, libraries were sequenced using standard Illumina oligos.

Sequencing

All sequencing was done at the UC-Berkeley Vincent J. Coates QB3 Sequencing Facility. Libraries were sequenced on an Illumina HiSeq 2500, 50SRR, with multiplexing.

Metabolomic profiling

Samples were harvested as follows: For Fig. S6A, BrÜn 10532 (*AID-HAC1 –TIR1*) and 10744 (*AID-HAC1 +TIR1*) were inoculated into YEPD and grown at 30C overnight, then diluted to OD_{600}0.05 in YEPD. After approximately 2.5 doublings, cultures were treated with 500μM auxin (Sigma) and 4μM IP_6 (Sigma). After 15 min, cultures were split into subcultures. Per strain, one subculture was not treated further (+auxin), and one was treated with 2μg/mL Tm (Calbiochem) (+auxin +Tm). After 2 hr, cultures were harvested by centrifugation (4C, 2,000 × g, 1 min), washed in cold water (4C, 15,000 × g, 30 sec), and flash frozen in ~30mg aliquots. Five technical replicates were collected per condition. For Fig. 6A, BrÜn 15 (WT) was used, except without the addition of auxin/IP6 and 6 technical replicates were collected per condition.

For both experiments, metabolomic analyses were performed as reported previously (Louie et al., 2016). Briefly, frozen cell pellets were resuspended with 150μL 40:40:20 acetonitrile/methanol/water containing 10nmoles D_3N^{15} serine internal standard (Cambridge isotopes). Samples were vortexed thoroughly for 30 sec and bath sonicated for 15 sec before centrifugation at 21,000 × g for 10 min. Supernatant was collected and frozen at −80° C until analysis. 20 ¼L of supernatant was analyzed by single-reaction monitoring (SRM)-based targeted LC-MS/MS. Separation of metabolites was performed by normal-phase chromatography using a Luna-5 mm NH2 column (50 mm × 4.60 mm, Phenomenex). Mobile phases were run as follows: Buffer A, acetonitrile; Buffer B, 95:5 water/ acetonitrile with 0.1% formic acid or 0.2% ammonium hydroxide with 50 mM ammonium acetate for positive and negative ionization modes, respectively. Flow rate began at 0.2 mL/min for 2 min, followed by a gradient starting at 0% B and increasing linearly to 100% B over the course of 13 min with a flow rate of 0.7 mL/min, followed by an isocratic gradient of 100% B for 10 min with a flow rate of 0.7mL/min before equilibrating for 5 min at 0% B with a flow rate of 0.7 mL/min. MS analysis was performed using an electrospray ionization (ESI) source on an Agilent 6430 QQQ LC-MS/MS. Capillary voltage was 3.0 kV, fragmentor voltage was 100 V, drying gas temperature 350° C, drying gas flow rate was 10 L/min, and the nebulizer pressure was 35 psi. Representative metabolites were quantified by SRM of the transitions from precursor to product ions at associated collision energies. Data was analyzed by calculating area under the curve using Agilent Qualitative Analysis software.

Author Manuscript Author Manuscript Author Manuscript Author Manuscript

Oxygen consumption assay

Except for materials needed for yeast cultures, all steps were carried out using components from a Seahorse Extracellular FluxPak (Agilent).

Preparation of cartridge: A Seahorse Extracellular Flux cartridge was hydrated with 200µl water per well overnight at 30C. Approximately 90 min prior to taking basal OCR measurements, water was removed and replaced with 200µl pre-warmed XF Calibrant solution.

Preparation of cell culture plate: Wells were coated with 20µl 0.1mg/mL poly-L-lysine (Sigma) for 10 min at RT. Poly-L-lysine was then removed and the plate allowed to dry before adding cells. Cells were grown and plated as follows. BrÜn 15 (WT) was inoculated into YEPD and grown at 30C overnight, then diluted to OD_{600}0.05 in YEPD. After ~2 doublings, cells were treated with 2µg/mL Tm (Calbiochem). This culture was used for the 6.5 hr Tm treatment samples. After 4.5 hr, an additional OD_{600}0.05 culture was started from the overnight inoculation, and after ~2 doublings, cells were treated with 2µg/mL Tm (Calbiochem) or vehicle. These cultures were used for the 2 hr Tm treatment samples and the control samples, respectively. After 6 hr and 1.5 hr, respectively, 0.3 OD units centrifuged at 1,500 × g, 2 min, RT. Cells were resuspended in 2 mL and then diluted 1:6 in fresh media (supplemented with Tm as appropriate). 180ul was added to each of 12 wells per condition. The plate was spun at 500 × g for 3 min at RT and then placed at 30C for 30 min. Immediately before OCR measurements, the plate was spun again as before.

OCR measurements: Following initial calibration, basal OCR was measured using a 2 min mix, 2 min measure protocol. Measurements, normalized to OD at the end of the assay, are reported in Fig. 6D.

Mass spectrometry

TMT-labeling and sample fractionation: Proteins were precipitated by adding −20°C cold acetone to the lysate (acetone to eluate ratio 10:1) and overnight incubation at −20°C. The proteins were pelleted by centrifugation at 20000xg for 15 min at 4°C. The supernatant was discarded and the pellet was left to dry by evaporation. The protein pellet was reconstituted in 100µl urea buffer (8M Urea, 75mM NaCl, 50mM Tris/HCl pH 8.0, 1mM EDTA), and protein concentrations were determined by BCA assay (Pierce). Fifteen µg of total protein per sample were processed further. Disulfide bonds were reduced with 5mM DTT and cysteines were subsequently alkylated with 10mM iodoacetamide. Samples were diluted 1:4 with 50mM Tris/HCl (pH 8.0) and sequencing grade modified trypsin (Promega) was added in an enzyme-to-substrate ratio of 1:50. After 16hr of digestion, samples were acidified with 1% formic acid (final concentration). Tryptic peptides were desalted on C18 StageTips according to (Rappsilber et al., 2007) and evaporated to dryness in a vacuum concentrator. Desalted peptides were labeled with the TMT11plex mass tag labeling reagent according to the manufacturer's instructions (Thermo Scientific) with small modifications. Briefly, 0.2units of TMT10plex reagent was used per 15µg of sample. Peptides were dissolved in 30µl of 50mM Hepes pH 8.5 solution and the TMT10plex reagent was added in 12.3µl of MeCN. After 1hr incubation, the reaction was stopped with 2.5µl 5%

Author Manuscript Author Manuscript Author Manuscript Author Manuscript

Hydroxylamine for 15min at 25°C. Differentially labeled peptides were mixed for each replicate (A-L were labeled with 126C, 127N, 127C, 128N, 128C, 129N, 129C, 130N, 130C, 131N, 131C, respectively) and subsequently desalted on C18 StageTips (Rappsilber et al., 2007) and evaporated to dryness in a vacuum concentrator.

The peptide mixtures were fractionated by Strong Cation Exchange (SCX) using StageTips as previously described (Rappsilber et al., 2007) with slight modifications. Briefly, one StageTip was prepared per sample by three SCX discs (3M, #2251) topped with two C18 discs (3M, #2215). The packed StageTips were first washed with 100µl methanol and then with 100µl 80% acetonitrile and 0.2% formic acid. Afterwards, they were equilibrated by 100µl 0.2% formic acid and the sample was loaded onto the discs. The sample was transeluted from the C18 discs to the SCX discs by applying 100µl 80% acetonitrile; 0.2% formic acid, which was followed by 3 stepwise elutions and collections of the peptide mix from the SCX discs. The first fraction was eluted with 50µl 50mM NH_4AcO; 20% MeCN (pH ~7.2), the second with 50µl 50mM NH_4HCO_3; 20% MeCN (pH ~8.5) and the sixth with 50µl 0.1% NH_4OH; 20% MeCN (pH ~9.5). 200µl of 0.2% acetic acid was added to each of the three fractions, and they were subsequently desalted on C18 StageTips as previously described (Rappsilber et al., 2007) and evaporated to dryness in a vacuum concentrator. Peptides were reconstituted in 10µl 0.2% formic acid. Both the unfractionated samples plus the fractionated, less complex samples were then analyzed by LC-MS/MS on a Q-Exactive HF was performed as previously described (Keshishian et al., 2015)

Approximately 1µg of total peptides was analyzed on an Eksigent nanoLC-415 HPLC system (Sciex) coupled via a 25cm C18 column (inner diameter of 100µm, packed in-house with 2.4µm ReproSil-Pur C18-AQ medium, Dr. Maisch GmbH) to a benchtop Orbitrap Q Exactive HF mass spectrometer (Thermo Fisher Scientific). Peptides were separated at a flow rate of 200nL/min with a linear 106min gradient from 2% to 25% solvent B (100% acetonitrile, 0.1% formic acid), followed by a linear 5min gradient from 25 to 85% solvent B. Each sample was run for 170min, including sample loading and column equilibration times. Data was acquired in data dependent mode using Xcalibur 2.8 software. MS1 Spectra were measured with a resolution of 60,000, an AGC target of 3E6 and a mass range from 375 to 2000m/z. Up to 15 MS2 spectra per duty cycle were triggered at a resolution of 60,000, an AGC target of 2E5, an isolation window of 1.6 m/z and a normalized collision energy of 36.

Label Free Quantification: In order to validate the TMT-based quantification results, we performed proteomics based on LFQ, which does the quantification on the MS1 level, instead of the MS2 level, and does not allow multiplexing as does TMT labeling. Therefore, different systematic biases are introduced by LFQ based proteomics than by TMT based proteomics, and it serves as a quite stringent test to our deep proteome quantification results obtained by our TMT based approach. We quantified all 11 matched samples.

Proteins were precipitated by adding −20°C cold acetone to the lysate (acetone to eluate ratio 10:1) and overnight incubation at −20°C. The proteins were pelleted by centrifugation at 20000xg for 15min at 4°C. The supernatant was discarded and the pellet was left to dry by evaporation. The protein pellet was reconstituted in 100µl urea buffer (8M Urea, 75mM

Author Manuscript Author Manuscript Author Manuscript Author Manuscript

NaCl, 50mM Tris/HCl pH 8.0, 1mM EDTA) and protein concentrations were determined by BCA assay (Pierce). 20μg of total protein per sample were processed further. Disulfide bonds were reduced with 5mM DTT and cysteines were subsequently alkylated with 10mM iodoacetamide. Samples were diluted 1:4 with 50mM Tris/HCl (pH 8.0) and sequencing grade modified trypsin (Promega) was added in an enzyme-to-substrate ratio of 1:50. After 16h of digestion, samples were acidified with 1% formic acid (final concentration). Tryptic peptides were desalted on C18 StageTips according to (Rappsilber et al., 2007) and evaporated to dryness in a vacuum concentrator. Desalted peptides were reconstituted in Buffer A (0.2% Formic acid).

LC-MS/MS analysis was performed on a Q-Exactive HF. Approximately 1μg of total peptides were analyzed on an Eksigent nanoLC-415 HPLC system (Sciex) coupled via a 25cm C18 column (inner diameter 100μm packed in-house with 2μm ReproSil-Pur C18-AQ medium, Dr. Maisch GmbH) to a benchtop Orbitrap Q Exactive HF mass spectrometer (Thermo Fisher Scientific). Peptides were separated at a flow rate of 200nL/min with a linear 106min gradient from 2% to 25% solvent B (100% acetonitrile, 0.1% formic acid), followed by a linear 5min gradient from 25 to 85% solvent B. Each sample was run for 170min, including sample loading and column equilibration times. Data was acquired in data dependent mode using Xcalibur 2.8 software. MS1 Spectra were measured with a resolution of 60,000, an AGC target of 3E6 and a mass range from 375 to 2000m/z. Up to 15 MS2 spectra per duty cycle were triggered at a resolution of 15,000, an AGC target of 2E5, an isolation window of 1.6 m/z and a normalized collision energy of 27.

QUANTIFICATION AND STATISTICAL ANALYSES

Sequence alignments and analysis

Performed as described in (Cheng et al., 2018), we observed the high technical and biological reproducibility that our lab typically observes using ribosome profiling and mRNA-sequencing. Plots are provided (Fig. S7) that exemplify this reproducibility. In the cases analyzed, we compared samples that should be biologically similar and that were harvested to provide additional controls within the experiment presented in Fig. 4A. Alignments were done using bowtie2 (Langmead and Salzberg, 2012). Genome browser analysis was done using Mochiview (Homann and Johnson, 2010). Cluster analysis and visualization were done using Cluster 3.0 and Java Treeview, respectively (de Hoon et al., 2004; Saldanha, 2004).

LUTI identification

mRNA-seq and ribosome profiling data for WT and *hac1Δ* cells, with either no treatment or treatment with DTT or Tm, as described above, were analyzed by genome browser (Mochiview). All annotated yeast genes were inspected visually for evidence of an alternate, 5’ extended transcript with translated uORFs that was Hac1- and UPR^{ER}-dependent. This approach was enabled by the simple transcript structures of most budding yeast genes. Of the ~30 candidates found by this approach, 19 showed an associated Hac1-dependent decrease in TE and were defined as candidate LUTIs. This set of 19 was reevaluated one-by-one in the AID-Hac1 experiment to determine if these hallmarks remained strong. In 15

Author Manuscript Author Manuscript Author Manuscript Author Manuscript

cases, this was true, and these genes are presented in Table 1. Note that a major caveat of this approach is that it is biased towards analysis of highly expressed mRNAs, as it is much more straightforward in these cases to detect the robust presence of alternate transcripts.

Translation efficiency calculations

TE values were obtained as described in (Ingolia et al., 2009). We calculated TE by dividing unfiltered footprint RPKMs by unfiltered mRNA RPKMs, summing reads over each annotated canonical ORF.

Statistical analyses

Hac1 target gene expression: We analyzed our sequencing and mass spectrometry data to determine if reported Hac1 targets (Travers et al., 2000) displayed the expected trends. In cases where we show changes in transcript or translation levels upon DTT or Tm treatment (Fig. 1C-D, 4B, S1A-B, S4D), we calculated the number of reported Hac1 targets up-regulated upon DTT or Tm treatment (fold-change $Y/X > 1$). We performed a resampling test (10,000 iterations) by taking subsamples from the overall gene set of size equal to the target gene set and calculating the number of up-regulated genes. P-values were determined from the frequency distribution of the number of up-regulated genes compared to the Hac1 target gene set. In cases where we show differences in transcript or translation levels between cells with and without Hac1 (Fig. 1E, S1C-D, S4A-C, S4E), we performed identical analyses using the inverse of the fold change (X/Y).

Metabolomics data: Reported p-values were generated by t-tests.

Oxygen consumption data: Reported p-values were generated by a two-tailed Mann-Whitney test.

Western blot quantification

Quantification of triplicate biological replicates was performed on raw images in Image Studio Lite (LI-COR). Signal intensity was normalized to that of a tubulin loading control.

Analysis of TMT mass spectrometry

All raw data were analyzed with MaxQuant software version 1.6.0.16 (Cox and Mann, 2008) using a UniProt yeast database (release 2014_09, strain ATCC 204508 / S288c), and MS/MS searches were performed with the following parameters: The five mass spec runs were grouped together. TMT11plex labeling on the MS2 level, oxidation of methionine and protein N-terminal acetylation as variable modifications; carbamidomethylation as fixed modification; Trypsin/P as the digestion enzyme; precursor ion mass tolerances of 20 p.p.m. for the first search (used for nonlinear mass re-calibration) and 4.5 p.p.m. for the main search, and a fragment ion mass tolerance of 20 p.p.m. For identification, we applied a maximum FDR of 1% separately on protein and peptide level. We required 1 or more unique/razor peptides for protein identification and a ratio count for each of the 11 TMT channels. This gave us a total of 2577 quantified protein groups.

Author Manuscript Author Manuscript Author Manuscript Author Manuscript

Finally, we normalized the MaxQuant generated corrected TMT intensities such that at each condition/time point the corrected TMT intensity values added up to exactly 1,000,000; therefore each protein group value can be regarded as a normalized microshare (we did this separately for each TMT channel for all proteins that made our filter cutoff in all the TMT channels).

Note: In order to compare protein group specific intensity values between the TMT quantified samples and our control label free quantified (LFQ) samples, we adjusted the normalization for the TMT data in order to incorporate the MS1 information as well. Each protein group of a TMT labeled sample got its proportional fraction of the MS1 based iBAQ intensities based on its labeling channel specific TMT MS2 intensity relative to the sum of TMT MS2 intensities of all labeled channels for the corresponding protein group. Afterwards we normalized these fractional MS1 iBAQ intensities such that at each condition/time point these intensity values added up to exactly 1,000,000, therefore each protein group value can be regarded as a normalized microshare. These microshare values are then comparable to the normalized microshare iBAQ based intensities from our label free samples (see below).

Analysis of LFQ mass spec

All raw data were analyzed with MaxQuant software version 1.6.0.1 (Cox and Mann, 2008) using a UniProt yeast database (release 2014_09, strain ATCC 204508 / S288c), and MS/MS searches were performed with the following parameters: Oxidation of methionine and protein N-terminal acetylation as variable modifications; carbamidomethylation as fixed modification; Trypsin/P as the digestion enzyme; precursor ion mass tolerances of 20 p.p.m. for the first search (used for nonlinear mass re-calibration) and 4.5 p.p.m. for the main search, and a fragment ion mass tolerance of 20 p.p.m. For identification, we applied a maximum FDR of 1% separately on protein and peptide level. “Match between the runs” was activated, as well as the “iBAQ” field. A total of 2475 protein groups was identified by at least 1 or more unique/razor peptides in any of the 11 samples. For any comparison between different samples only protein groups that had been assigned iBAQ values in each of the samples that were used.

Finally, we normalized the MaxQuant generated iBAQ intensities such that at each condition/time point the iBAQ intensity values added up to exactly 1,000,000; therefore each protein group value can be regarded as a normalized microshare (we did this separately for each sample for all proteins that were present in that sample).

DATA AND SOFTWARE AVAILABILITY

All sequencing data can be accessed at NCBI GEO with accession number GSE115366. Mass spectrometry data are available on the MassIVE platform with accession number MSV000082454.

Supplementary Material

Refer to Web version on PubMed Central for supplementary material.

Author Manuscript Author Manuscript Author Manuscript Author Manuscript

Acknowledgements:

Thanks to Jonathan Weissman, James Olzmann, Elcin Unal, and Andy Dillin for helpful comments on the manuscript. Thanks to Erica Moehle and the Dillin lab for use of and assistance with their Seahorse XF analyzer, and to members of the Brar and Ünal labs, Christopher Mugler, and Leon Chan for experimental suggestions. We thank Mark Rose for the generous gift of the Kar2 antibody to the Br-Ün lab. This work was funded by the NIH (DP2-GM-119138), investigator awards from the Alfred P. Sloan Foundation and Pew Charitable Trusts, and UC-Berkeley start-up funding to GAB. DKN and CAB are funded by NIH/NCI grant R01CA172667. MJ, SH, and AK are funded by Columbia start-up funding. KMV and AH were funded by NSF pre-doctoral fellowships (DGE1106400 and DGE 1106400/1752814, respectively). KMV, AH, and GMO were also funded by NIH training grants to the MCB department (T32 GM 0007232 and T32 HG 00047).

References:

Aragón T, van Anken E, Pincus D, Serafimova IM, Korennykh AV, Rubio CA, and Walter P (2009). Messenger RNA targeting to endoplasmic reticulum stress signalling sites. Nature 457, 736–740. [PubMed: 19079237]

Bowring CE, and Llewellyn DH (2001). Differences in HAC1 mRNA processing and translation between yeast and mammalian cells indicate divergence of the eukaryotic ER stress response. Biochem. Biophys. Res. Commun. 287, 789–800. [PubMed: 11563865]

Chan LY, Mugler CF, Heinrich S, Vallotton P, and Weis K (2017). Non-invasive measurement of mRNA decay reveals translation initiation as the major determinant of mRNA stability. bioRxiv 10.1101/214775.

Chapman R, Sidrauski C, and Walter P (1998). Intracellular signaling from the endoplasmic reticulum to the nucleus. Annu. Rev. Cell Dev. Biol. 14, 459–485. [PubMed: 9891790]

Chen J, Tresenrider A, Chia M, McSwiggen DT, Spedale G, Jorgensen V, Liao H, van Werven FJ, and Unal E (2017). Kinetochore inactivation by expression of a repressive mRNA. eLife 6.

Cheng Z, Otto GM, Powers EN, Keskin A, Mertins P, Carr S, Jovanovic M, and Brar GA (2018). Pervasive, coordinated protein level changes driven by transcript isoform switching during meiosis. Cell 172, 910–923. [PubMed: 29474919]

Chia M, Tresenrider A, Chen J, Spedale G, Jorgensen V, Unal E, and van Werven FJ (2017). Transcription of a 5' extended mRNA isoform directs dynamic chromatin changes and interference of a downstream promoter. eLife 6.

Church C, Chapon C, and Poyton RO (1996). Cloning and characterization of PET100, a gene required for the assembly of yeast cytochrome c oxidase. J. Biol. Chem. 271, 18499–18507. [PubMed: 8702496]

Cox J, and Mann M (2008). MaxQuant enables high peptide identification rates, individualized p.p.b.-range mass accuracies and proteome-wide protein quantification. Nat. Biotechnol. 26, 1367–1372. [PubMed: 19029910]

Cox JS, and Walter P (1996). A novel mechanism for regulating activity of a transcription factor that controls the unfolded protein response. Cell 87, 391–404. [PubMed: 8898193]

Cullen BR, Lomedico PT, and Ju G (1984). Transcriptional interference in avian retroviruses--implications for the promoter insertion model of leukaemogenesis. Nature 307, 241–245. [PubMed: 6363938]

Haghighat A, Svitkin Y, Novoa I, Kuechler E, Skern T, and Sonenberg N (1996). The eIF4G-eIF4E complex is the target for direct cleavage by the rhinovirus 2A proteinase. J. Virol. 70, 8444–8450. [PubMed: 8970966]

Han J, and Kaufman RJ (2017). Physiological/pathological ramifications of transcription factors in the unfolded protein response. Genes Dev. 31, 1417–1438. [PubMed: 28860159]

Hell K, Tzagoloff A, Neupert W, and Stuart RA (2000). Identification of Cox20p, a novel protein involved in the maturation and assembly of cytochrome oxidase subunit 2. J. Biol. Chem. 275, 4571–4578. [PubMed: 10671482]

Hinnebusch AG (1993). Gene-specific translational control of the yeast GCN4 gene by phosphorylation of eukaryotic initiation factor 2. Mol. Microbiol. 10, 215–223. [PubMed: 7934812]

Author Manuscript Author Manuscript Author Manuscript Author Manuscript

Hollien J, Lin JH, Li H, Stevens N, Walter P, and Weissman JS (2009). Regulated Ire1-dependent decay of messenger RNAs in mammalian cells. J. Cell Biol. 186, 323–331. [PubMed: 19651891]

Homann OR, and Johnson AD (2010). MochiView: versatile software for genome browsing and DNA motif analysis. BMC Biol. 8, 49. [PubMed: 20409324]

De Hoon MJL, Imoto S, Nolan J, and Miyano S (2004). Open source clustering software. Bioinforma. Oxf. Engl. 20, 1453–1454.

Ingolia NT, Ghaemmaghami S, Newman JRS, and Weissman JS (2009). Genome-wide analysis in vivo of translation with nucleotide resolution using ribosome profiling. Science 324, 218–223. [PubMed: 19213877]

Jonikas MC, Collins SR, Denic V, Oh E, Quan EM, Schmid V, Weibezahn J, Schwappach B, Walter P, Weissman JS, et al. (2009). Comprehensive characterization of genes required for protein folding in the endoplasmic reticulum. Science 323, 1693–1697. [PubMed: 19325107]

Keshishian H, Burgess MW, Gillette MA, Mertins P, Clauser KR, Mani DR, Kuhn EW, Farrell LA, Gerszten RE, and Carr SA (2015). Multiplexed, Quantitative Workflow for Sensitive Biomarker Discovery in Plasma Yields Novel Candidates for Early Myocardial Injury. Mol. Cell. Proteomics MCP 14, 2375–2393. [PubMed: 25724909]

Kiss DL, Waters CE, Ouda IM, Saldivar JC, Karras JR, Amin ZA, Mahrous S, Druck T, Bundschuh RA, Schoenberg DR, et al. (2017a). Identification of Fhit as a post-transcriptional effector of Thymidine Kinase 1 expression. Biochim. Biophys. Acta 1860, 374–382. [PubMed: 28093273]

Kiss DL, Baez W, Huebner K, Bundschuh R, and Schoenberg DR (2017b).Impact of FHIT loss on the translation of cancer-associated mRNAs. Mol. Cancer 16, 179. [PubMed: 29282095]

Krishnan K, Ren Z, Losada L, Nierman WC, Lu LJ, and Askew DS (2014). Polysome profiling reveals broad translatome remodeling during endoplasmic reticulum (ER) stress in the pathogenic fungus Aspergillus fumigatus. BMC Genomics 15, 159. [PubMed: 24568630]

Labunskyy VM, Gerashchenko MV, Delaney JR, Kaya A, Kennedy BK, Kaeberlein M, and Gladyshev VN (2014). Lifespan extension conferred by endoplasmic reticulum secretory pathway deficiency requires induction of the unfolded protein response. PLoS Genet. 10, e1004019. [PubMed: 24391512]

Langmead B, and Salzberg SL (2012). Fast gapped-read alignment with Bowtie 2. Nat. Methods 9, 357–359. [PubMed: 22388286]

Law GL, Bickel KS, MacKay VL, and Morris DR (2005). The undertranslated transcriptome reveals widespread translational silencing by alternative 5' transcript leaders. Genome Biol. 6, R111. [PubMed: 16420678]

Lee JE, Oney M, Frizzell K, Phadnis N, and Hollien J (2015). Drosophila melanogaster activating transcription factor 4 regulates glycolysis during endoplasmic reticulum stress. G3 Bethesda Md 5, 667–675.

Lee K, Neigeborn L, and Kaufman RJ (2003). The unfolded protein response is required for haploid tolerance in yeast. J. Biol. Chem. 278, 11818–11827. [PubMed: 12560331]

Longtine MS, McKenzie A, Demarini DJ, Shah NG, Wach A, Brachat A, Philippsen P, and Pringle JR (1998). Additional modules for versatile and economical PCR-based gene deletion and modification in Saccharomyces cerevisiae. Yeast Chichester Engl. 14, 953–961.

Louie SM, Grossman EA, Crawford LA, Ding L, Camarda R, Huffman TR, Miyamoto DK, Goga A, Weerapana E, and Nomura DK (2016). GSTP1 Is a Driver of Triple-Negative Breast Cancer Cell Metabolism and Pathogenicity. Cell Chem. Biol. 23, 567–578. [PubMed: 27185638]

Martens JA, Laprade L, and Winston F (2004). Intergenic transcription is required to repress the Saccharomyces cerevisiae SER3 gene. Nature 429, 571–574. [PubMed: 15175754]

Maurel M, Chevet E, Tavernier J, and Gerlo S (2014). Getting RIDD of RNA: IRE1 in cell fate regulation. Trends Biochem. Sci. 39, 245–254. [PubMed: 24657016]

Metzger MB, and Michaelis S (2008). Analysis of Quality Control Substrates in Distinct Cellular Compartments Reveals a Unique Role for Rpn4p in Tolerating Misfolded Membrane Proteins. Mol. Biol. Cell 20, 1006–1019. [PubMed: 19073890]

Mori K, Kawahara T, Yoshida H, Yanagi H, and Yura T (1996). Signalling from endoplasmic reticulum to nucleus: transcription factor with a basic-leucine zipper motif is required for the unfolded protein-response pathway. Genes Cells 1, 803–817. [PubMed: 9077435]

Author Manuscript Author Manuscript Author Manuscript Author Manuscript

Moseley JL, Page MD, Alder NP, Eriksson M, Quinn J, Soto F, Theg SM, Hippler M, and Merchant S (2002). Reciprocal Expression of Two Candidate DiIron Enzymes Affecting Photosystem I and Light-Harvesting Complex Accumulation. Plant Cell 14, 673–688. [PubMed: 11910013]

Nishimura K, Fukagawa T, Takisawa H, Kakimoto T, and Kanemaki M (2009). An auxin-based degron system for the rapid depletion of proteins in nonplant cells. Nat. Methods 6, 917–922. [PubMed: 19915560]

Ogawa N, and Mori K (2004). Autoregulation of the HAC1 gene is required for sustained activation of the yeast unfolded protein response. Genes Cells Devoted Mol. Cell. Mech. 9, 95–104.

Otto GM, and Brar GA (2018). Seq-ing answers: uncovering the unexpected in global gene regulation. Curr. Genet.

Patil CK, Li H, and Walter P (2004). Gcn4p and novel upstream activating sequences regulate targets of the unfolded protein response. PLoS Biol. 2, E246. [PubMed: 15314660]

Payne T, Hanfrey C, Bishop AL, Michael AJ, Avery SV, and Archer DB (2008). Transcript-specific translational regulation in the unfolded protein response of *Saccharomyces cerevisiae*. FEBS Lett. 582, 503–509. [PubMed: 18206654]

Rappsilber J, Mann M, and Ishihama Y (2007). Protocol for micro-purification, enrichment, pre-fractionation and storage of peptides for proteomics using StageTips. Nat Protoc. 2, 1896–1906. [PubMed: 17703201]

Saldanha AJ (2004). Java Treeview--extensible visualization of microarray data. Bioinforma. Oxf. Engl. 20, 3246–3248.

Sathe L, Bolinger C, Mannan MA, Dever TE, and Dey M (2015). Evidence That Base-pairing Interaction between Intron and mRNA Leader Sequences Inhibits Initiation of HAC1 mRNA Translation in Yeast. J. Biol. Chem. 290, 21821–21832. [PubMed: 26175153]

Schuldiner M, and Weissman JS (2013). The Contribution of Systematic Approaches to Characterizing the Proteins and Functions of the Endoplasmic Reticulum. Cold Spring Harb. Perspect. Biol. 5, a013284–a013284. [PubMed: 23359093]

Sehgal A, Hughes BT, and Espenshade (2008). Oxygen-dependent, alternative promoter controls translation of tco1 + in fission yeast. Nucleic Acids Res. 36, 2024–2031. [PubMed: 18276645]

Seraphin B (1992). The HIT protein family: a new family of proteins present in prokaryotes, yeast and mammals. DNA Seq. J. DNA Seq. Mapp. 3, 177–179.

Sidrauski C, Cox JS, and Walter P (1996). tRNA ligase is required for regulated mRNA splicing in the unfolded protein response. Cell 87, 405–413. [PubMed: 8898194]

Titov DV, Cracan V, Goodman RP, Peng J, Grabarek Z, and Mootha VK (2016). Complementation of mitochondrial electron transport chain by manipulation of the NAD+/NADH ratio. Science 352, 231–235. [PubMed: 27124460]

Travers KJ, Patil CK, Wodicka L, Lockhart DJ, Weissman JS, and Walter P (2000). Functional and genomic analyses reveal an essential coordination between the unfolded protein response and ER-associated degradation. Cell 101, 249–258. [PubMed: 10847680]

Tresenrider A, and Unal E (2017). One-two punch mechanism of gene repression: a fresh perspective on gene regulation. Curr. Genet.

Vander Heiden MG, Cantley LC, and Thompson CB (2009). Understanding the Warburg effect: the metabolic requirements of cell proliferation. Science 324, 1029–1033. [PubMed: 19460998]

Walter P, and Ron D (2011). The unfolded protein response: from stress pathway to homeostatic regulation. Science 334, 1081–1086. [PubMed: 22116877]

Warburg O (1956). On the Origin of Cancer Cells. Science 123, 309–314. [PubMed: 13298683]

Wenger CD, Lee MV, Hebert AS, McAlister GC, Phanstiel DH, Westphall MS, and Coon JJ (2011). Gas-phase purification enables accurate, multiplexed proteome quantification with isobaric tagging. Nat. Methods 8, 933–935. [PubMed: 21963608]

Author Manuscript Author Manuscript Author Manuscript Author Manuscript

Highlights

- Yeast Hac1/XBP1 coordinate up- and down-regulation of distinct protein sets for UPR^{ER}
- Repression occurs via mechanism of alternative transcription start site usage (LUTI)
- Hac1 directs proteome remodeling in UPR^{ER} and influences cellular metabolism control
- Altering cellular respiration improves UPR^{ER}-activated cell fitness

Author Manuscript Author Manuscript Author Manuscript Author Manuscript

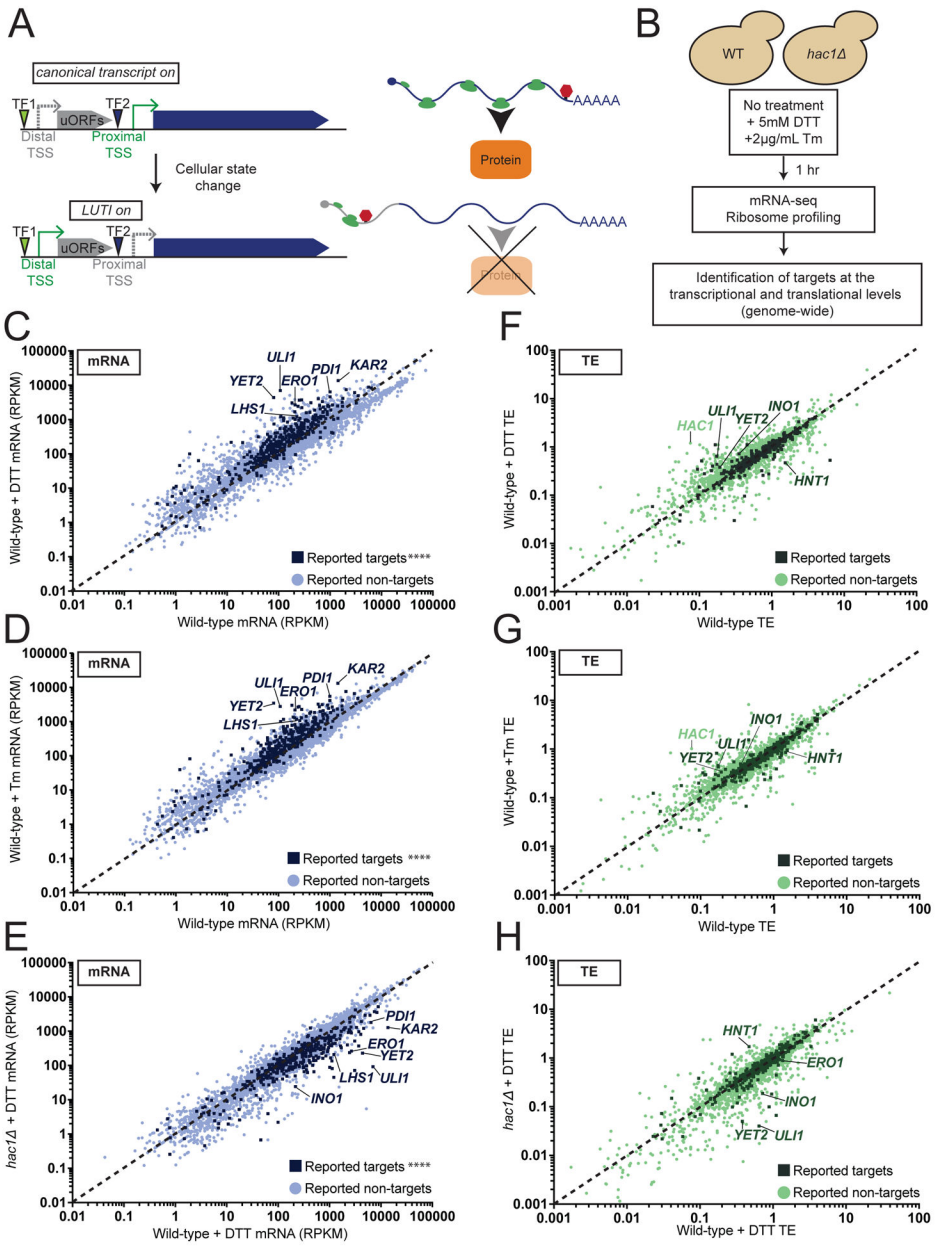

Figure 1. Global analysis of *HAC1*-dependent changes in gene expression during the UPR^{ER}.

(A) Schematic of LUTI-mediated repression of gene expression. (B) Harvesting scheme to compare mRNA and translation levels in WT and *hac1Δ* cells. (C-E) Comparison of mRNA levels in cells with and without activation of an intact UPR^{ER}. Reported Hac1 targets were significantly (****p<0.0001) more likely to be up-regulated in a Hac1-dependent manner upon UPR^{ER} induction than the full gene set. F-H) Comparison of TEs for each gene with and without activation of an intact UPR^{ER}. Note that for C-H previously reported Hac1 targets (Travers et al., 2000) are shown with dark squares while all other genes are shown with light circles. See also Fig. S1 and Tables S1-S2.

Author Manuscript Author Manuscript Author Manuscript Author Manuscript

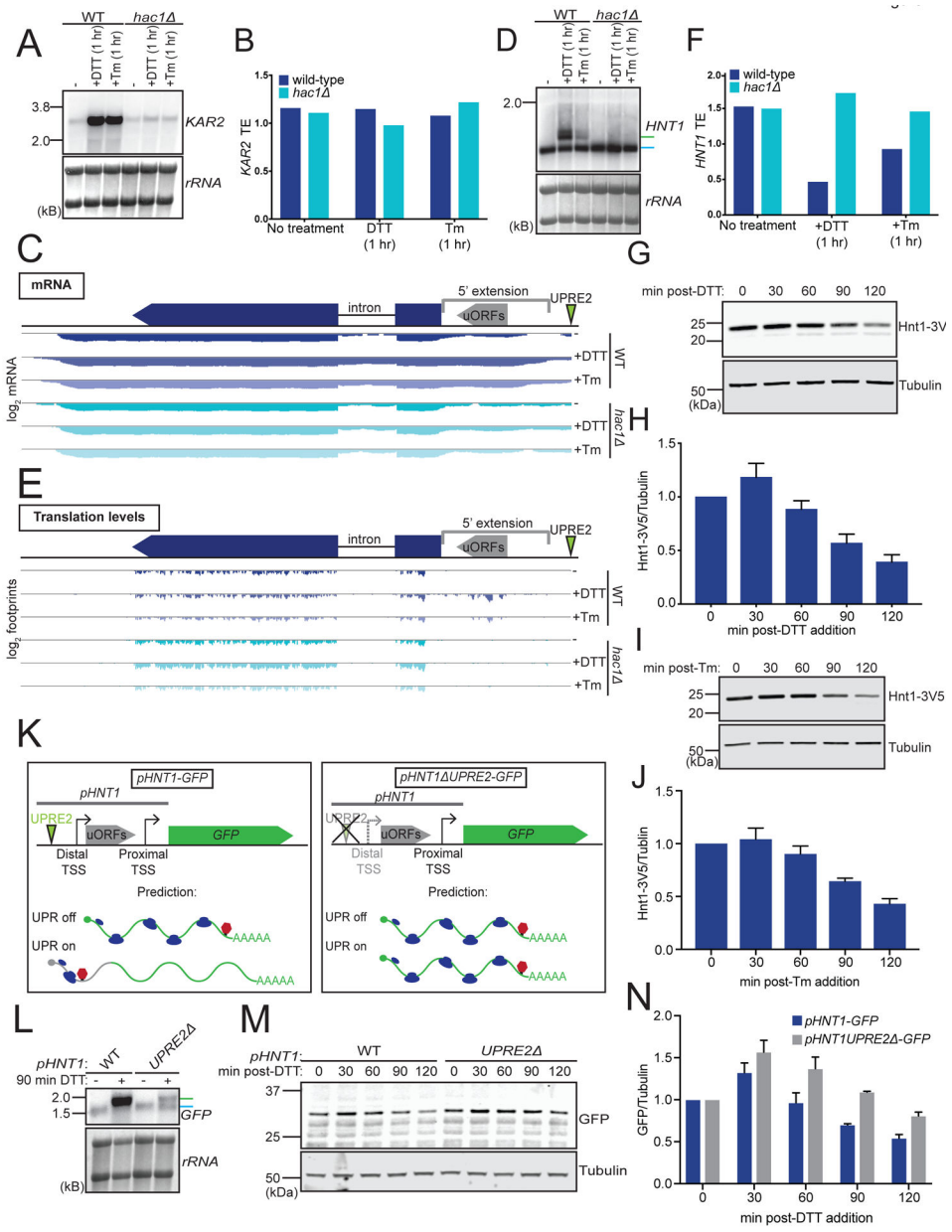

Figure 2. *HAC1*-dependent transcription of an alternate transcript isoform is correlated with decreased protein levels.

(A) Northern blotting for *KAR2* shows the abundance of a single transcript isoform increases upon UPR^{ER} activation, dependent on *HAC1*. B) Comparison of *KAR2* TEs with and without UPR activation. C) Annotation of *HNT1* mRNA expression during the UPR^{ER}. Above, gene model. Below, $\log_2$ mRNA (RPKM) showing an extension in transcript length upon UPR^{ER} activation in WT cells. D) Northern blotting for *HNT1* reveals an extended transcript isoform is produced upon UPR^{ER} activation, dependent on *HAC1*. Blue and green bars highlight canonical and extended transcripts, respectively. E) Annotation of *HNT1* translation during the UPR^{ER}. Above, gene model. Below, $\log_2$ footprints (RPKM) showing translation of uORFs in the extended transcript. F) Comparison of *HNT1* TEs with and

Author Manuscript Author Manuscript Author Manuscript Author Manuscript

without UPR activation. G-J) A decrease in Hnt1-3V5 protein was observed upon UPR^{ER} activation with DTT (G-H) or Tm (I-J). Quantifications represent the average of 3 biological replicates with error bars representing SD. K) GFP reporters were constructed in order to assess the role of the UPRE2 in the *HNT1* distal promoter. L) Northern blotting for *GFP* shows a longer transcript isoform is produced upon UPR^{ER} induction, but expression of the longer isoform is strongly reduced when the UPRE2 motif is disrupted. Blue and green bars highlight canonical and extended transcripts, respectively. M-N) A decrease in GFP protein was observed upon UPR^{ER} induction in cells harboring *pHNT1-GFP*, but was less efficient in cells harboring *pHNT1ΔUPRE2-GFP*. Quantification represents the average of 3 biological replicates with error bars representing SD. See also Figs. S2-S3.

Author Manuscript Author Manuscript Author Manuscript Author Manuscript

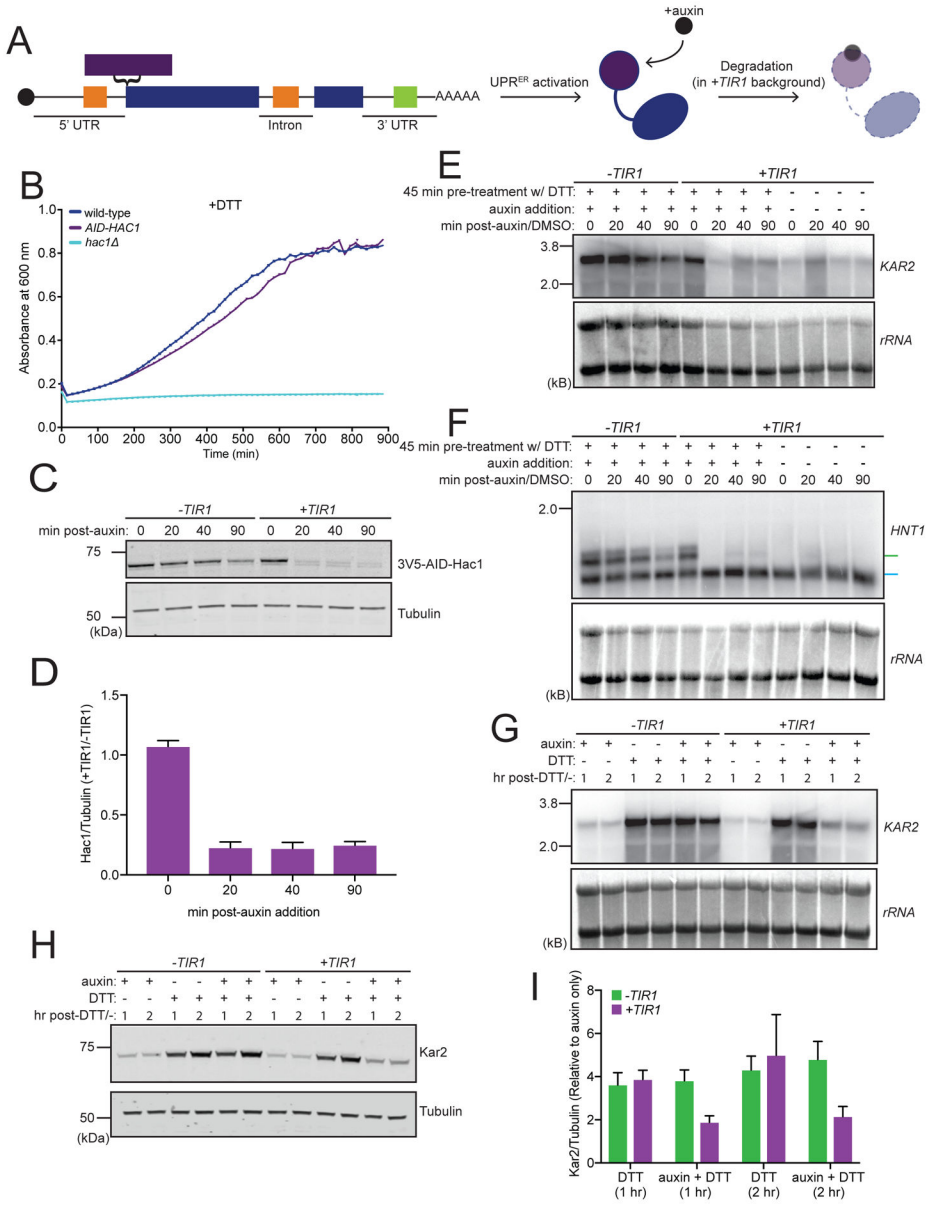

Figure 3. AID-Hac1 is functional and its degradation results in observable changes in the levels of Hac1 targets.

A) Schematic of the *AID-HAC1* allele. Regions of the 5' UTR and intron that participate in base-pairing (BP) to repress translation were unperturbed, and the 3' targeting element (TE) remained intact. B) *AID-HAC1* rescues the growth defect of *hac1Δ* in DTT. C-D) AID-Hac1 (anti-3V5) is efficiently degraded within 20 min of auxin addition following 45 min DTT pre-treatment. Quantification represents the average of 3 biological replicates with error bars representing SD. E) Northern blotting for *KAR2* indicates that transcripts for canonical Hac1 targets decrease within 20 min of auxin addition following 45 min DTT pre-treatment. F) Northern blotting for *HNT1* reveals that *HNT1*^{LUTI} behaves in the same manner as *KAR2* (panel E) upon treatment with auxin following 45 min DTT pre-treatment. Blue and green bars highlight canonical and extended transcripts, respectively. G) Pre-treating cells with

Author Manuscript Author Manuscript Author Manuscript Author Manuscript

auxin for 15 min prevents increased *KAR2* expression upon subsequent treatment with DTT. H-I) The effect of pre-treating cells with auxin for 15 min prior to DTT treatment manifests in observable changes in Kar2 protein levels. Quantification represents the average of 3 biological replicates with error bars representing SD. See also Fig. S2.

Author Manuscript Author Manuscript Author Manuscript Author Manuscript

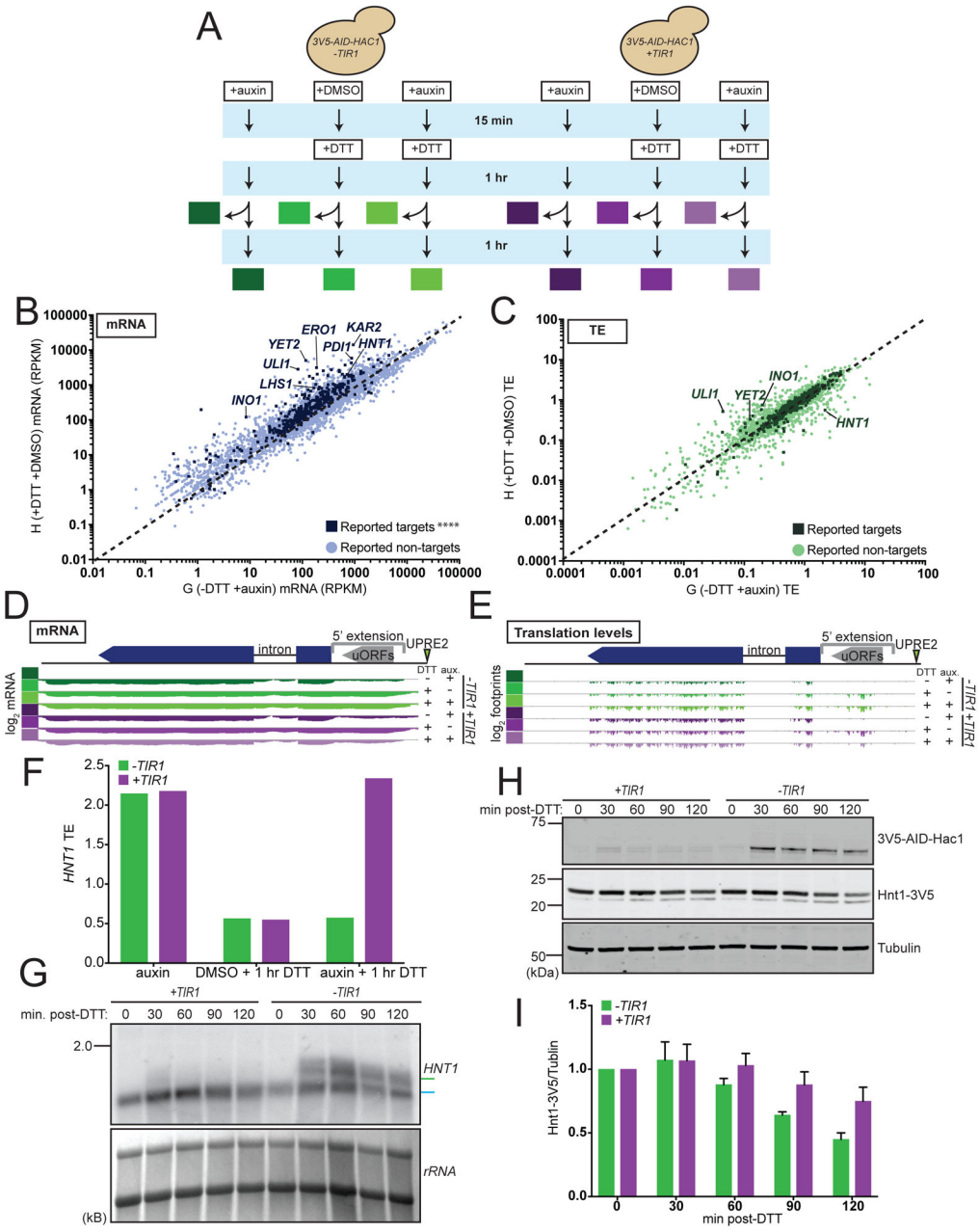

Figure 4. Global analysis of UPR^{ER}-dependent changes in gene expression in the *AID-HAC1* background

A) Schematic of harvesting scheme. B) Comparison of mRNA levels in cells with and without DTT treatment in the *AID-HAC1* background. Reported Hac1 targets were significantly (****p<0.0001) more likely to be upregulated upon UPR^{ER} induction than the full gene set. C) Comparison of TEs for each gene with and without DTT treatment in the *AID-HAC1* background. Note that for panels (B-C), previously reported Hac1 targets (Travers et al., 2000) are shown with dark squares while all other genes are shown with light circles. D) Annotation of *HNT1* mRNA expression in the *AID-HAC1* background during the UPR*ER*. Above, gene model. Below, $\log_2$ mRNA (RPKM) showing a Hac1 dependent

Author Manuscript Author Manuscript Author Manuscript Author Manuscript

HNT1 transcript extension upon UPR^{ER} induction. E) Annotation of *HNT1* translation in the *AID-HAC1* background during the UPR^{ER}, as determined by the experiment described in panel A. Above, gene model. Below, log_2 footprints (RPKM) showing translation of uORFs in $HNT1^{LUTI}$. F) Comparison of *HNT1* TEs across samples A-C and G-I. G) Northern blot analysis of $HNT1^{LUTI}$ mRNA expression with and without Hac1 degradation. Blue and green bars highlight canonical and extended transcripts, respectively. H-I) Western blot showing Hac1 dependent reduction in Hnt1-3V5 protein levels upon treatment with DTT (following 15 min auxin pre-treatment). Quantification represents the average of 3 biological replicates with error bars representing SD. See also Figs. S2 and S4.

Author Manuscript Author Manuscript Author Manuscript Author Manuscript

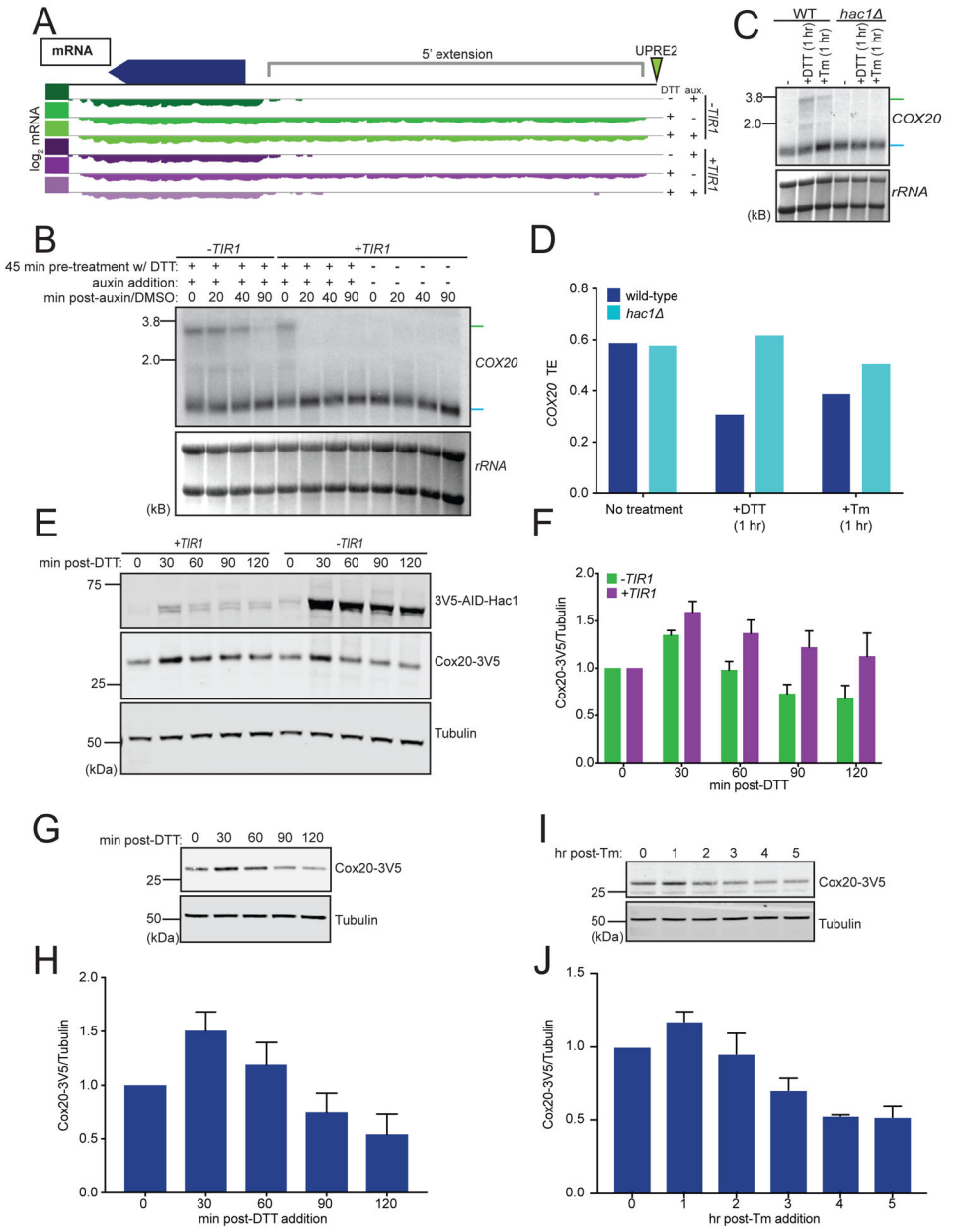

Figure 5. Cox20 protein levels are down-regulated by a Hac1-dependent LUTI mechanism.

A) Annotation of *COX20* mRNA expression during the UPR^{ER}, as determined by the experiment described in Fig. 4A. Above, gene model. Below, $\log_2$ mRNA (RPKM) showing an extension in *COX20* transcript length upon UPR*ER* activation in cells not depleted of Hac1. B) Northern blotting for *COX20* confirms expression of an extended transcript isoform, which decreases within 20 min of auxin addition following 45 min DTT pre-treatment. Blue and green bars highlight canonical and extended transcripts, respectively. C) The extended *COX20* transcript was also observed in WT cells upon treatment with DTT or Tm, but not *hac1Δ* cells. Blue and green bars highlight canonical and extended transcripts, respectively. D) Comparison of *COX20* TEs with and without UPR activation. E-F) Western blot showing Hac1-dependent reduction in Cox20-3V5 protein levels upon treatment with

Author Manuscript Author Manuscript Author Manuscript Author Manuscript

DTT (following 15 min auxin pre-treatment). Quantification represents the average of 3 biological replicates with error bars representing SD. G-I) A decrease in Cox20-3V5 protein in WT cells was observed by western blot upon UPR^{ER} activation with DTT (G-H) or Tm (I-J). Quantifications represent the average of 3 biological replicates with error bars representing SD. See also Figs. S2 and S5.

Author Manuscript Author Manuscript Author Manuscript Author Manuscript

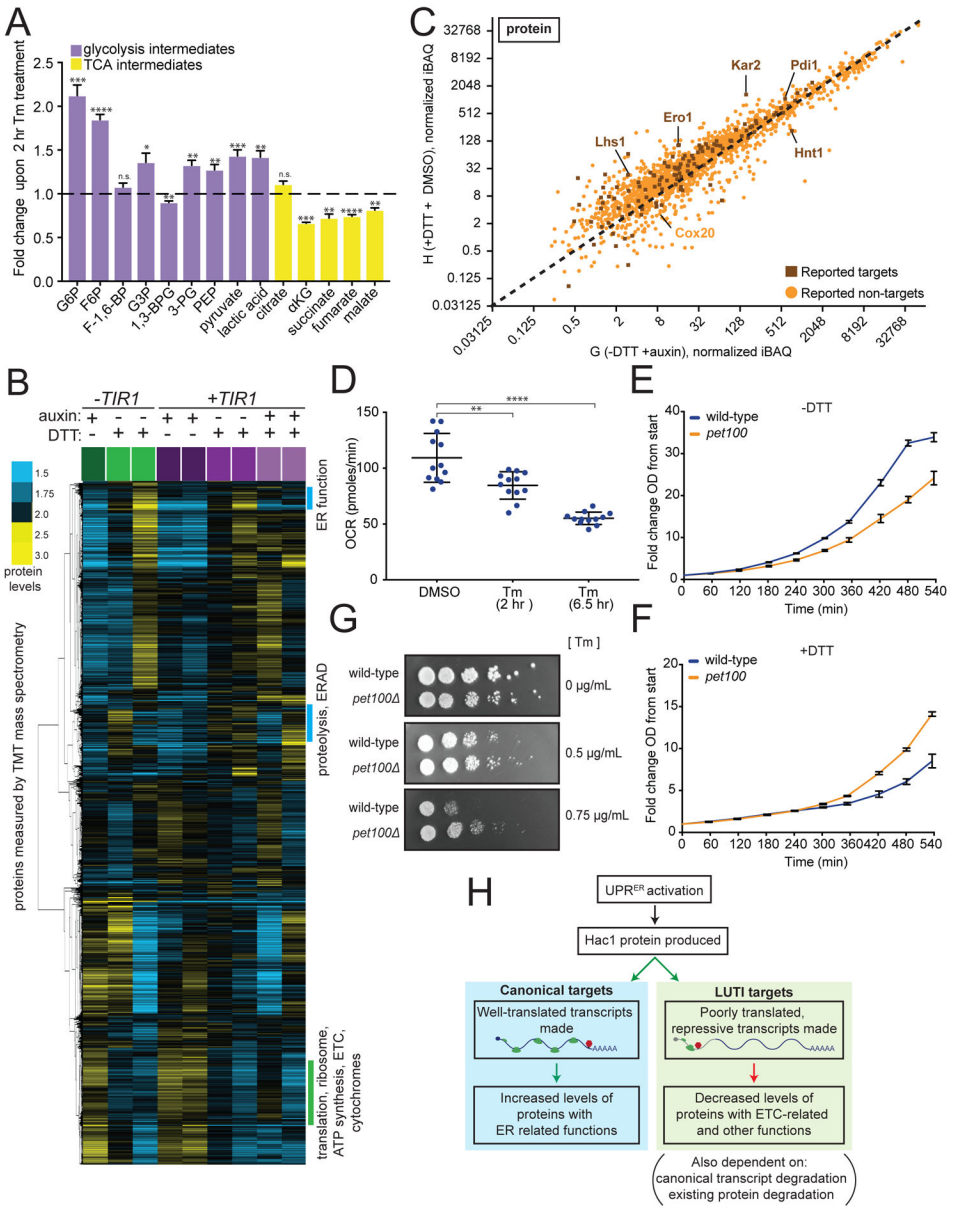

Figure 6. Induction of the UPR^{ER} results in coordinated up- and down-regulation of distinct protein classes and promotes a metabolic shift.

A) Metabolite levels following Tm treatment of WT cells. Average fold change of 6 technical replicates is shown, with error bars representing SEM. A t-test was used to evaluate significance. *p<0.05, **p<0.01, ***p<0.001, ****p<0.0001. B) Proteins quantified by TMT-based mass spectrometry are clustered by abundance patterns, with each normalized to the same total protein level across the row to enable comparison of trends. Proteins involved in ER function, proteolysis, and ERAD appear to be up-regulated in a Hac1 dependent manner (blue bars). Proteins involved in translation, ribosome biogenesis, ATP synthesis, the ETC, and cytochromes appear to be down-regulated in a Hac1 dependent manner (green bar). C) Protein levels obtained via label-free mass spectrometry analysis are plotted with previously reported Hac1 transcriptional targets shown in dark squares. D)

Author Manuscript Author Manuscript Author Manuscript Author Manuscript

Basal OCRs were measured following treatment of WT cells with Tm. Rates from replicate wells are plotted, with overlaid bars representing average and SD. Rates were adjusted to normalize for OD differences. A Mann-Whitney test was used to statistically compare OCR. **p<0.01, ****p<0.0001. E-F) Growth of WT and *pet100Δ* cells with and without DTT. Fold change in OD relative to the starting OD is plotted against time. G) Serial dilution-based growth assay of WT and *pet100Δ* cells on plates containing 0-0.75μg/mL Tm. H) Model for Hac1-coordinated up- and down-regulation during the UPR^{ER}. See also Fig. S6 and Tables S3-S6.

Author Manuscript Author Manuscript Author Manuscript Author Manuscript

Table 1:

Hac1-dependent LUTI candidates. Systematic analysis of mRNA-seq and TE data from WT and *hac1Δ* cells (Fig. 1B) was used to predict LUTI candidates. Nineteen candidates were identified. Re-analysis of these same features using the *AID-HAC1* allele (Fig. 4A) confirmed 15 of these candidates, and many were previously reported to show decreased translation upon Tm addition (Labunskyy et al., 2014).

		Wild-type/*hac1Δ* dataset		*AID-HAC1* dataset		
Gene	**Full name**	**HAC1-dependent decrease in TE**	**Hac1-dependent extended transcript**	**Hac1-dependent decrease in TE**	**Hac1-dependent extended transcript**	**Monosome shifted upon DTT addition[a]**
COX20	Cytochrome c OXidase	+	+	+	+	+
HNT1	Histidine triad Nucleo Tidebinding	+	+	+	+	+
MSK1	Mitochondrial aminoacyl-tRNA Synthetase, lysine(K)	+	+	+	+	−
SOM1	SOrting Mitochondrial	+	+	+	+	+
GTT1	GlutaThione Transferase	+	+	+	+	+
IRC4	Increased Recombination Centers	+	+	+	+	+
CRR1	CRH-Related	+	+	+	+	−
HEM1	HEMe biosynthesis	+	+	+	+	+
OXA1	cytochrome OXidase Activity	+	+	+[c]	+	+
NRG2	Negative Regulator of Glucose-controlled genes	+	+	+[c]	+	−
YPL067C	Histidine Triad with Channel	+	+	+	+	−
SRM1	Suppressor of Receptor Mutations	+	+	+	+	+
CTS1	ChiTinaSe	+	+	+[c]	+	−
PCM1	PhosphoaCetylglucosamine Mutase	+	+	+	+	+
YHB1	Yeast flavoHemogloBin	+	+	+	+	+
FLR1[d]	FLuconazole Resistance	+	+	−	+	−
PRY1[d]	Pathogen Related in Yeast	+	+[b]	+[c]	+[b]	−
SRL1[d]	Suppressor of Rad53 null Lethality	+	+	+[c]	+[b]	−
SET2[d]	SET domain-containing	+	+	−	+	−

[a] As reported in (Payne et al., 2008)

[b] Difficult to definitively call for reasons including locus complexity

[c] Hac1-dependence inconclusive

[d] Called as LUTI candidates in WT/*hac1Δ* but not *AID-HAC1*